nature cell biology

The TDH–GCN5L1–Fbxo15–KBP axis limits mitochondrial biogenesis in mouse embryonic stem cells

Valerio Donato[1,2,3], Massimo Bonora[4], Daniele Simoneschi[1,2], Davide Sartini[1,2,9], Yasusei Kudo[1,2,5], Anita Saraf[6], Laurence Florens[6], Michael P. Washburn[6,7], Matthias Stadtfeld[8], Paolo Pinton[4] and Michele Pagano[1,2,3,10]

Self-renewing naive mouse embryonic stem cells (mESCs) contain few mitochondria, which increase in number and volume at the onset of differentiation. KBP (encoded by *Kif1bp*) is an interactor of the mitochondrial-associated kinesin Kif1Bα. We found that TDH, responsible for mitochondrial production of acetyl-CoA in mESCs, and the acetyltransferase GCN5L1 cooperate to acetylate Lys501 in KBP, allowing its recognition by and degradation via Fbxo15, an F-box protein transcriptionally controlled by the pluripotency core factors and repressed following differentiation. Defects in KBP degradation in mESCs result in an unscheduled increase in mitochondrial biogenesis, enhanced respiration and ROS production, and inhibition of cell proliferation. Silencing of Kif1Bα reverts the aberrant increase in mitochondria induced by KBP stabilization. Notably, following differentiation, *Kif1bp*$^{-/-}$ mESCs display impaired expansion of the mitochondrial mass and form smaller embryoid bodies. Thus, KBP proteolysis limits the accumulation of mitochondria in mESCs to preserve their optimal fitness, whereas KBP accumulation promotes mitochondrial biogenesis in differentiating cells.

Mitochondria are dynamic double-membrane organelles that take part in essential cellular functions, such as aerobic energy production, cell signalling, apoptosis and calcium homeostasis[1,2]. The total mitochondrial content of a cell and the individual activity of each mitochondrion differ from cell type to cell type due to variations in energy requirements. For example, naive mouse embryonic stem cells (mESCs)—characterized by indefinite self-renewal and wide developmental potency—and differentiated cells vary in their mitochondrial content and activity. Although they perform both glycolysis and oxidative phosphorylation, naive mESCs display a poor repertoire of mitochondria with immature morphology. The fine tuning of mitochondrial content and function in naive mESCs is necessary, at least in part, to minimize the production of reactive oxygen species (ROS)[3]. Following differentiation, mESCs leave their self-renewal state and expand their mitochondrial network in a process called mitochondrial biogenesis, which is required to adapt to changes in cellular metabolism, volume and shape[3–6]. While it is well established that transcription factors, such as PGC-1α and NRF-2, contribute to mitochondrial biogenesis[7,8], little is known about the role of the ubiquitin–proteasome system in controlling the mitochondrial network of mESCs.

Among the targets of transcription factors essential for mESCs such as Oct-3/4 and Sox2, *Fbxo15* gained attention as it was originally used to isolate induced pluripotent stem cells[9,10]. *Fbxo15* encodes Fbxo15, one member of more than 70 mammalian F-box proteins, which are the substrate recognition subunits of the SCF (Skp1–Cul1–F-box protein) ubiquitin ligase complexes[11,12]. Fbxo15 is unique among the F-box protein family due to its strict mESC expression; however, the function of Fbxo15 in mESCs has remained elusive.

Here, we describe Kif1-binding protein (KBP) as a substrate of Fbxo15 in mESCs. In humans, KBP is encoded by the *KIAA1279* gene, which is mutated in the Goldberg–Shprintzen syndrome, an

[1]Department of Biochemistry and Molecular Pharmacology, New York University School of Medicine, 522 First Avenue, SRB 1107, New York, New York 10016, USA. [2]NYU Perlmutter Cancer Center, New York University School of Medicine, 522 First Avenue, SRB 1107, New York, New York 10016, USA. [3]Howard Hughes Medical Institute, New York University School of Medicine, 522 First Avenue, SRB 1107, New York, New York 10016, USA. [4]Department of Morphology, Surgery and Experimental Medicine, University of Ferrara, Via Fossato di Mortara 70, Ferrara 44121, Italy. [5]Department of Oral Molecular Pathology, Tokushima University Graduate School 3-18-15 Kuramoto, Tokushima 770-8504, Japan. [6]The Stowers Institute for Medical Research, 1000 East 50th Street, Kansas City, Missouri 64110, USA. [7]Department of Pathology and Laboratory Medicine, The University of Kansas Medical Center, 3901 Rainbow Boulevard, Kansas City, Kansas 66160, USA. [8]Skirball Institute of Biomolecular Medicine and Helen L. and Martin S. Kimmel Center for Biology and Medicine, New York University School of Medicine, 522 First Avenue, New York, New York 10016, USA. [9]Present address: Department of Clinical Sciences and Department of Life and Environmental Sciences, Polytechnic University of Marche, Via Brecce Bianche, Ancona 60131, Italy.
[10]Correspondence should be addressed to M.P. (e-mail: michele.pagano@nyumc.org)

Received 16 January 2017; accepted 13 February 2017; published online 20 March 2017; DOI: 10.1038/ncb3491

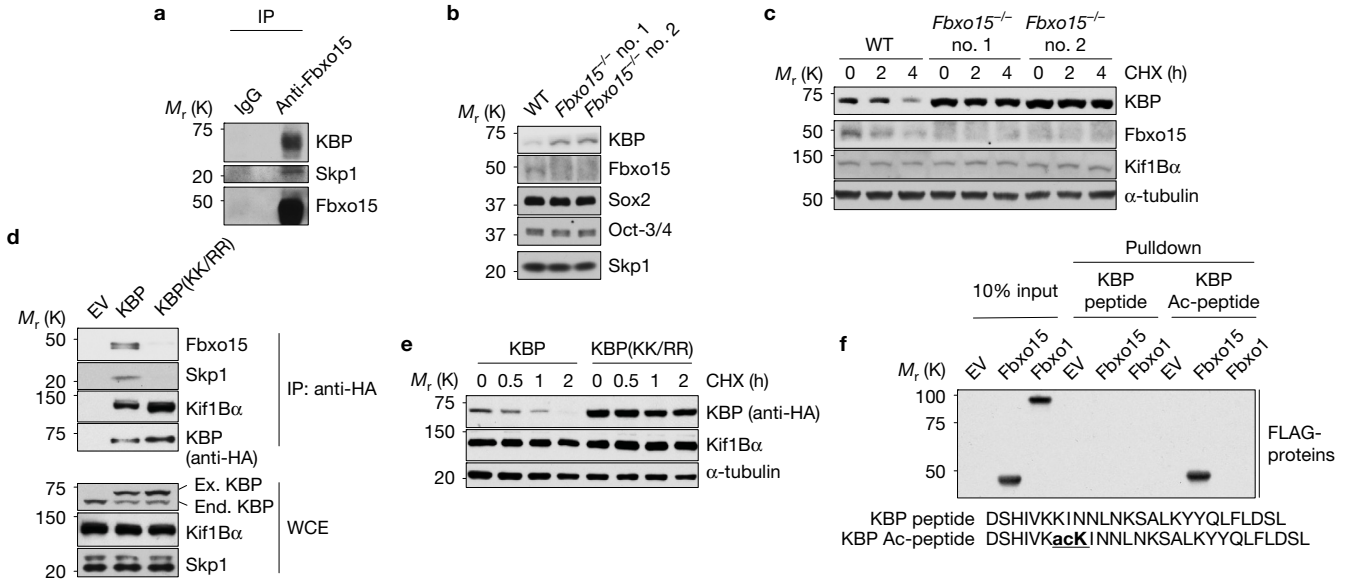

Figure 1 KBP is an Fbxo15 substrate that is recognized in an acetylation-dependent manner. (**a**) Self-renewing, naive mESCs were treated with MG132 for 4 h prior to lysis. Lysates were immunoprecipitated (IP) with either an affinity-purified polyclonal antibody against Fbxo15 or an affinity-purified rabbit IgG, and analysed by immunoblotting as indicated. (**b**) Protein extracts from wild-type (WT) mESCs and *Fbxo15*$^{-/-}$ mESCs (two different clones) were immunoblotted for the indicated proteins. (**c**) *Fbxo15*$^{-/-}$ mESCs (two different clones) were treated with cycloheximide (CHX) for the indicated times, after which cell extracts were immunoblotted for the indicated proteins. This experiment was performed twice. (**d**) mESCs were infected with either an empty virus (EV) or lentiviruses expressing haemagglutinin (HA)-tagged wild-type mouse KBP or HA-tagged mouse KBP(KK/RR). Whole-cell extracts (WCE) were immunoprecipitated with an anti-HA resin, and proteins were immunoblotted as indicated. Ex., exogenous; End., endogenous. (**e**) mESCs were infected with lentiviruses expressing either HA-tagged WT mouse KBP or HA-tagged mouse KBP(KK/RR), treated with CHX for the indicated times, and total cell lysates were analysed by immunoblotting as indicated. (**f**) *In vitro*-translated FLAG-tagged Fbxo15 and FLAG-tagged Fbxo1 were incubated with beads coupled to the indicated peptides. Beads were extensively washed, and bound proteins were immunoblotted with an anti-FLAG antibody. Unprocessed original scans of blots are shown in Supplementary Fig. 9. Unless otherwise noted, experiments were performed at least three times.

autosomal recessive disorder characterized by neuronal defects, such as microcephaly and mega-colon[13]. At the cellular level, this disorder is characterized by defects in axonal growth, which can be recapitulated by the expression of mutants of *kif1bp* (the orthologue of *KIAA1279*) in zebrafish[14]. KBP was originally characterized as an interactor of the kinesin Kif1Bα, a motor protein responsible for anterograde mitochondrial transportation[15,16]. Nonetheless, additional reports[17,18] challenged the concept of KBP as a mediator of axonal mitochondrial transportation. Moreover, KBP expression is not limited to neurons, but is ubiquitous and is detected during all developmental stages, albeit at different levels.

Through biochemical, morphological and functional analyses combined with genetics, we characterized the biological significance of KBP degradation, elucidating a critical control mechanism that limits mitochondrial mass expansion in self-renewing mESCs. The results of these studies are presented below.

RESULTS

Fbxo15 binds acetylated KBP and targets it for degradation in mESCs

To identify substrates recognized by Fbxo15, we transiently expressed Strep-FLAG-tagged Fbxo15 and Strep-FLAG-tagged Fbxo21 (the latter used as control) in HEK293T cells. Fbxo15 and Fbxo21 complexes were then immunopurified for analysis by Multidimensional Protein Identification Technology (MudPIT), which revealed that Fbxo15 interacted with KBP, Cul1 and Skp1 (Supplementary Fig. 1a and Supplementary Table 1). In contrast, Fbxo21 interacted with Cul1 and Skp1, but not with KBP.

We verified the ability of Fbxo15 to specifically bind endogenous KBP in HEK293T using a collection of other F-box proteins as controls (Supplementary Fig. 1b). Moreover, the interaction between endogenous KBP and endogenous Fbxo15 was confirmed in naive mESCs (Fig. 1a).

The knockdown of Fbxo15 resulted in increased levels of KBP in mESCs maintained under self-renewing conditions (Supplementary Fig. 1c) to an extent comparable to that observed when mESCs were treated with the proteasome inhibitor MG132 (Supplementary Fig. 1d). The effects of Fbxo15 depletion and proteasome inhibition were not synergistic, indicating that they work in the same pathway. Moreover, silencing of Fbxo15 by two distinct short interfering RNA (siRNA) oligonucleotides, used individually, prolonged the half-life of KBP (Supplementary Fig. 1e and, later, Fig. 2b). Similarly, mESCs in which both alleles of *Fbxo15* were eliminated using a CRISPR/Cas9-dependent strategy (Supplementary Fig. 1f) also displayed elevated levels and increased stability of KBP (Fig. 1b,c). These results suggest that Fbxo15 targets KBP for proteasomal degradation in self-renewing mESCs.

In most instances, F-box proteins recognize substrates only when one or two residues in their 'degron' (that is, the degradation motif) are phosphorylated[11]. To identify the degron in KBP that is required

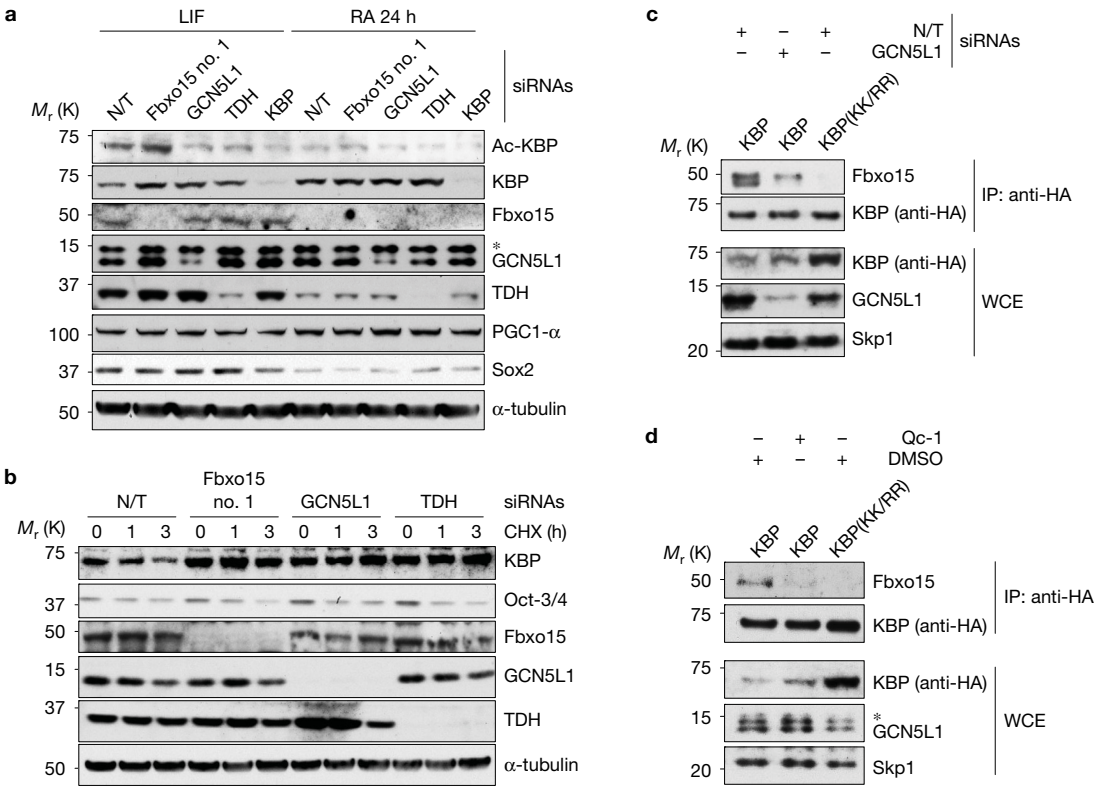

Figure 2 GCN5L1 and TDH are necessary for the Fbxo15-mediated degradation of KBP in mESCs. (**a**) mESCs were transfected with either a non-targeting (N/T) siRNA or siRNAs against Fbxo15 (oligo no. 1), GCN5L1, TDH or KBP. Cells were either maintained in leukaemia inhibitory factor (LIF)-containing medium or induced to differentiate for 24 h after LIF withdrawal and exposure to retinoic acid (RA). Cells were then collected and lysed for immunoblotting as indicated. The asterisk denotes a nonspecific band. (**b**) mESCs were transfected with a non-targeting (N/T) siRNA or siRNAs against Fbxo15 (oligo no. 2), GCN5L1 or TDH and treated with cycloheximide (CHX) for the indicated times. Cells were then collected and lysed for immunoblotting as indicated. (**c**) mESCs were infected with lentiviruses expressing either HA-tagged WT mouse KBP or HA-tagged mouse KBP(KK/RR) and then transfected with the indicated siRNAs. Whole-cell extracts (WCE) were immunoprecipitated (IP) with an anti-HA resin, and immunocomplexes were probed with antibodies against the indicated proteins. (**d**) mESCs were infected with lentiviruses expressing either HA-tagged WT mouse KBP or HA-tagged mouse KBP(KK/RR) and then treated for 12 h with either DMSO or Qc-1. Whole-cell extracts (WCE) were immunoprecipitated (IP) with anti-HA resin, and immunocomplexes were probed with antibodies against the indicated proteins. The asterisk denotes a nonspecific band. Unprocessed original scans of blots are shown in Supplementary Fig. 9. Unless otherwise noted, experiments were performed at least three times.

for its interaction with Fbxo15, we generated a number of human KBP deletion mutants and identified a highly conserved stretch of 24 amino acids that is necessary for Fbxo15 binding (Supplementary Fig. 2a–f). We mutated all potential phospho-sites in this region (Ser500, Ser512, Tyr516, Tyr517 and Ser523) to alanine, either individually or in different combinations, but no mutation impaired the binding of KBP to Fbxo15 (Supplementary Fig. 2a–f). Further characterization of this 24-amino-acid region by alanine-scanning mutagenesis showed that mutation of Lys505 to alanine (K505A), but not K504A, abolished the binding of KBP to Fbxo15 (Supplementary Fig. 2b–d and f–g). Mutation of Lys505 to arginine partially impaired the binding to Fbxo15 (perhaps due to a compensatory effect of Lys504), but mutations of Lys505 and Lys504 (KBP(KK/RR)) rendered KBP completely unable to interact with Fbxo15 (Supplementary Fig. 2f,g).

Human and mouse KBP share 91.5% identity and 96% similarity. The inability of KBP(KK/RR) to bind endogenous Fbxo15 was confirmed in mESCs that were infected with lentiviruses expressing either wild-type mouse KBP or mouse KBP(KK/RR) (the latter generated by mutating Lys500 and Lys501, corresponding to human Lys504 and Lys505, to arginine) (Fig. 1d). Importantly, mouse KBP(KK/RR) displayed a much longer half-life than that of wild-type KBP (Fig. 1e).

Fbxo15 appears to interact with the Kif1Bα-free pool of KBP, since it did not co-precipitate Kif1Bα (Supplementary Fig. 1b). Moreover, KBP mutants unable to interact with Fbxo15 still bound Kif1Bα efficiently (Supplementary Fig. 2b,d). Similarly, the stable KBP(KK/RR) mutant co-precipitated more Kif1Bα from mESCs, compared with the less abundant wild-type KBP (Fig. 1d). The last experiment shows that when free KBP is not degraded through Fbxo15, the fraction of KBP associated with Kif1Bα increases.

We also analysed the post-translational modifications of immunopurified KBP by mass spectrometry. This analysis revealed that Lys505 is acetylated in vivo (Supplementary Fig. 2h). Next, we used immobilized, synthetic peptides containing the candidate acetylated degron sequence to test its binding to Fbxo15. Whilst the immobilized peptide containing acetylated Lys505 efficiently pulled down Fbxo15 (but not Fbxo1 used as control), the corresponding

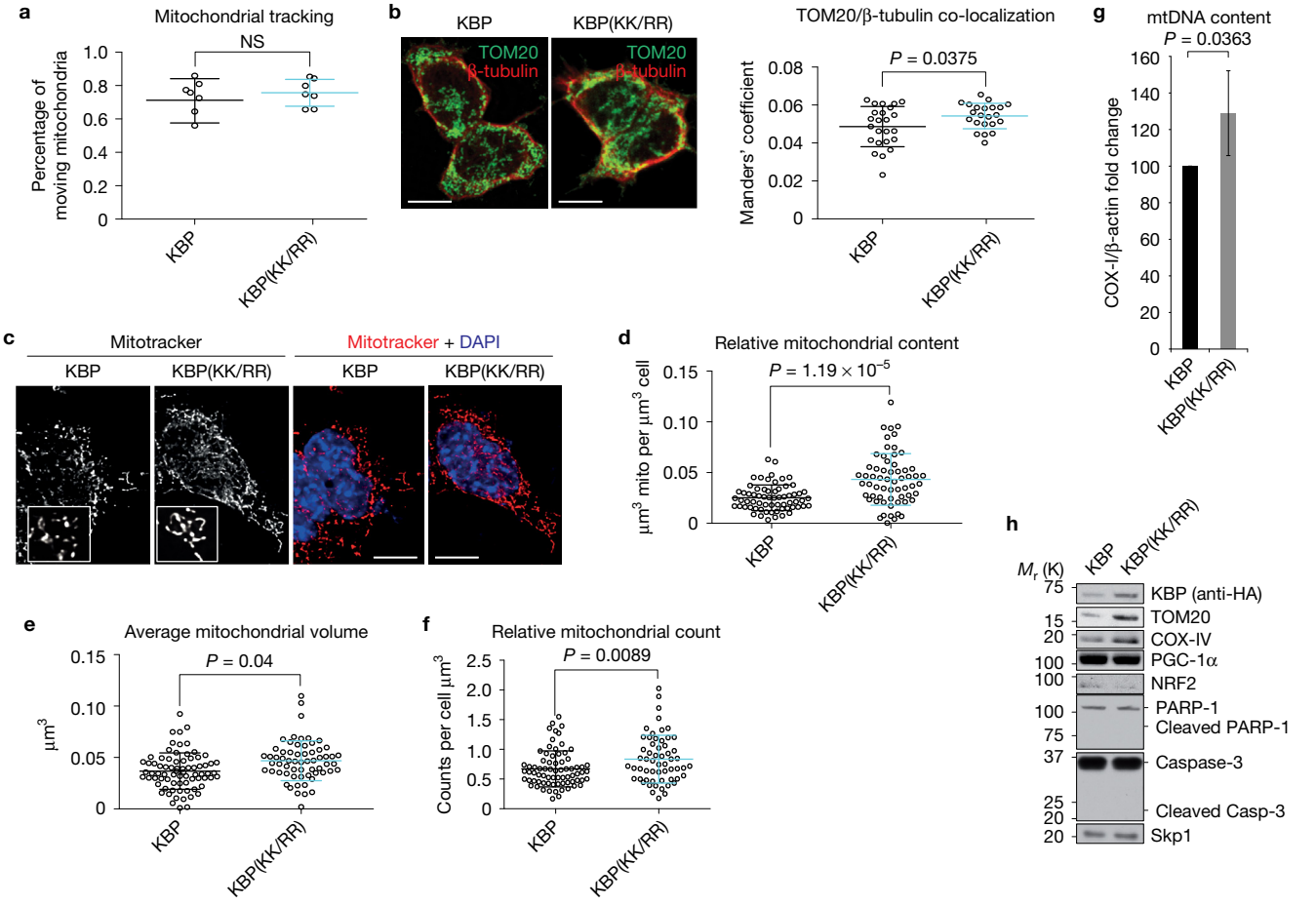

Figure 3 Expression of a stable mutant of KBP in mESCs induces mitochondrial biogenesis. (**a**) mESCs stably infected with lentiviruses expressing either HA-tagged WT mouse KBP or HA-tagged mouse KBP(KK/RR) were transfected with mitochondria-targeted GFP and monitored with live-cell imaging. The graph shows the percentage of moving mitochondria per cell. $n=7$ independent field acquisitions. *P* value was calculated by unpaired *t*-test. Error bars indicate ± s.d. This experiment was performed once. NS, not significant. (**b**) Cells as in **a** were immunostained for TOM20 and β-tubulin. Microtubule–mitochondria co-localization was detected by confocal microscopy. Scale bars, 15 μm. The graph (right) shows Manders' overlap coefficient. $n=24$ and 22 (KBP and KBP(KK/RR), respectively). *P* value was calculated by *t*-test. Error bars indicate ± s.d. (**c**–**f**) Cells as in **a** were stained with Mitotracker and DAPI. 3D images were collected through widefield microscopy and reconstructed by 3D deconvolution. Panel **c** shows representative maximum intensity projections (MIPs) of the mitochondrial network of KBP- and KBP(KK/RR)-expressing mESCs. Scale bars, 15 μm. KBP- and KBP(KK/RR)-expressing mESCs were compared for their relative mitochondrial content (**d**), average mitochondrial volume (**e**), and number of mitochondria per cell (**f**). $n=65$ and 60 (KBP and KBP(KK/RR), respectively). *P* values were calculated by unpaired *t*-test. Error bars indicate ± s.d. (**g**) mESCs were infected with lentiviruses expressing either HA-tagged WT mouse KBP or HA-tagged mouse KBP(KK/RR). After completing the selection process, total cellular DNA was extracted and mitochondrial DNA (mtDNA) copy number was evaluated by qPCR normalized using β-actin DNA copy number. mtDNA amount in mESCs expressing WT KBP was set as 100 and the graph shows the fold change. *P* value was calculated by unpaired *t*-test. Error bars indicate ± s.d. $n=4$ biologically independent experiments (see Supplementary Table 6). (**h**) mESCs stably infected with lentiviruses expressing either HA-tagged WT mouse KBP or HA-tagged mouse KBP(KK/RR) were collected and lysed for immunoblotting as indicated. Unprocessed original scans of blots are shown in Supplementary Fig. 9. Unless otherwise noted, experiments were performed at least three times.

non-acetylated peptide was unable to bind Fbxo15 (Fig. 1f). Collectively, our results indicate that acetylation of the KBP degron at Lys505 is required for its interaction with Fbxo15. To date, no other SCF substrate degron has been shown to contain an acetylated motif[11].

GCN5L1- and TDH-mediated acetylation of KBP is required for its recognition by Fbxo15 in mESCs

To further investigate KBP acetylation *in vivo*, we generated an acetyl-specific antibody against the acetylated degron motif. This antibody recognized wild-type KBP, but not KBP(KK/RR) (Supplementary Fig. 2i), confirming that KBP is acetylated *in vivo* on Lys505. Notably, depletion of Fbxo15 in mESCs induced an increase in the levels of KBP acetylated on Lys501 (the murine equivalent of Lys505) (Fig. 2a and Supplementary Fig. 3a), providing further support for the degradation of acetyl-KBP via Fbxo15.

To date, two mitochondrial acetyltransferases have been reported: ACAT1 (acetyl-CoA acetyltransferase 1) and GCN5L1 (general control nonrepressed 5-like 1). ACAT1 is involved in ketone body metabolism and is localized inside the mitochondrial matrix[19], whereas GCN5L1 is also localized to the cytoplasm, suggesting that it may be present on the outer mitochondrial membrane[20]. Moreover,

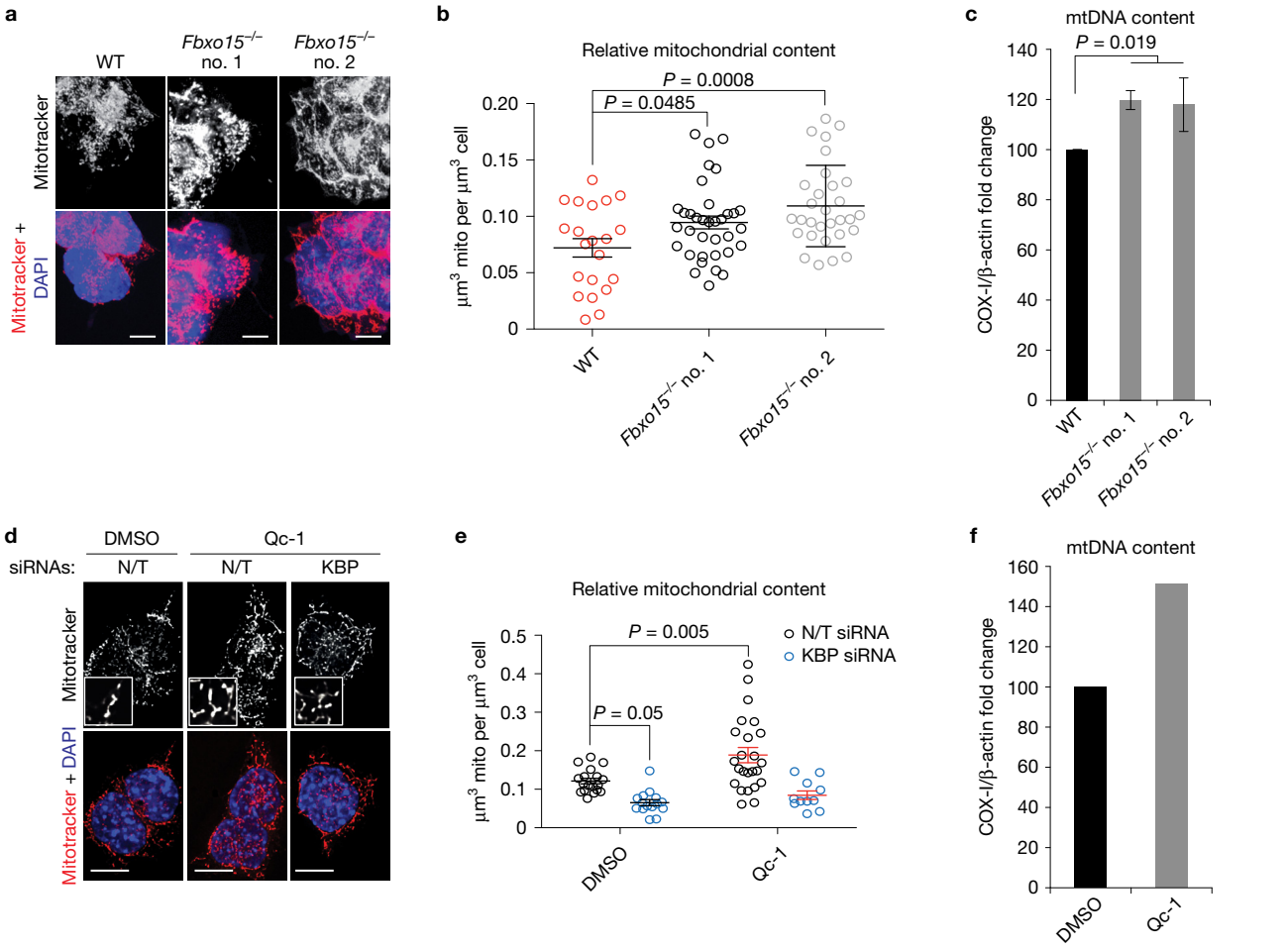

Figure 4 Failure to degrade KBP in mESCs induces mitochondrial biogenesis. (**a**,**b**) WT mESCs and *Fbxo15*$^{-/-}$ mESCs (two different clones) were maintained in self-renewing conditions. Cells were stained with Mitotracker and DAPI prior to fixation and then analysed by confocal microscopy. Panel **a** shows the MIPs of representative cells (scale bars, 15 µm). Panel **b** shows the quantification of the relative mitochondrial content. $n=21$, 35 and 30 cells (WT, *Fbxo15*$^{-/-}$ no. 1 and *Fbxo15*$^{-/-}$ no. 2, respectively). *P* value was calculated by one-way ANOVA. Error bars indicate ± s.d. (**c**) WT mESCs and *Fbxo15*$^{-/-}$ mESCs (two different clones) were maintained in self-renewing conditions. Total cellular DNA was extracted and mtDNA copy number was evaluated by qPCR normalized using β-actin DNA copy number. mtDNA amount in WT mESCs was set as 100 and the graph shows the fold change. *P* value was calculated by one-way ANOVA. Error bars indicate ± s.d. $n=3$ biologically independent experiments (see Supplementary Table 6). (**d**,**e**) mESCs were transfected with either a non-targeting (N/T) siRNA or an siRNA to KBP, and then incubated with either DMSO or Qc-1 for 12 h. Cells were stained with Mitotracker and DAPI prior to fixation and then analysed by confocal microscopy. Panel **d** shows the MIPs of representative cells (scale bars, 15 µm). Panel **e** shows the quantification of average mitochondrial content. $n=19$, 15, 24 and 11 cells (N/T siRNA+DMSO, KBP siRNA+DMSO, N/T siRNA+Qc-1, and KBP siRNA+Qc-1, respectively). This experiment was performed twice. *P* value was calculated by two-way ANOVA. Error bars indicate ± s.d. (**f**) mESCs were treated with DMSO or Qc-1 for 12 h. Total cellular DNA was extracted and mtDNA copy number was evaluated by qPCR normalized using β-actin DNA copy number. mtDNA amount in mESCs treated with vehicle (DMSO) was set as 100 and the graph shows the fold change. $n=2$ biologically independent experiments with three technical replicates each (see Supplementary Table 6).

GCN5L1 plays a role in the remodelling and biogenesis of mitochondria and other organelles[21,22]. Thus, we tested the hypothesis that GCN5L1 may acetylate KBP. Indeed, silencing of GCN5L1 in mESCs reduced the levels of acetyl-KBP (Lys501), whilst simultaneously increasing the total levels of KBP (Fig. 2a and Supplementary Fig. 3a; compare lanes 1 and 3) and prolonging its half-life (Fig. 2b). Importantly, knockdown of GCN5L1 in mESCs resulted in a dramatic reduction in the binding between KBP and Fbxo15 (Fig. 2c), supporting the hypothesis that GCN5L1 promotes this protein–protein interaction by acetylating KBP.

During mESC self-renewal, the production of acetyl-CoA (coenzyme A) at the mitochondria requires the activity of TDH (L-threonine dehydrogenase)[23], and it is assumed that this event is solely required for channelling acetyl-CoA into the tricarboxylic acid cycle and the synthesis of *S*-adenosylmethionine[23,24]. Similar to Fbxo15[9], levels of TDH are downregulated in primed pluripotent stem cells and following the induction of differentiation of mESCs[23–26]. To study the role of TDH in KBP acetylation and stability in mESCs, we depleted its expression by siRNA and observed both less acetylation of KBP on Lys501 and an increase in KBP levels and stability (Fig. 2a,b). Short treatment of mESCs with Qc-1, a pharmacological inhibitor of TDH that impairs the production of acetyl-CoA in mESCs[27], resulted in an increase of both KBP protein level and half-life (Supplementary Fig. 3b,c). Moreover, we found that Qc-1 treatment abrogated the

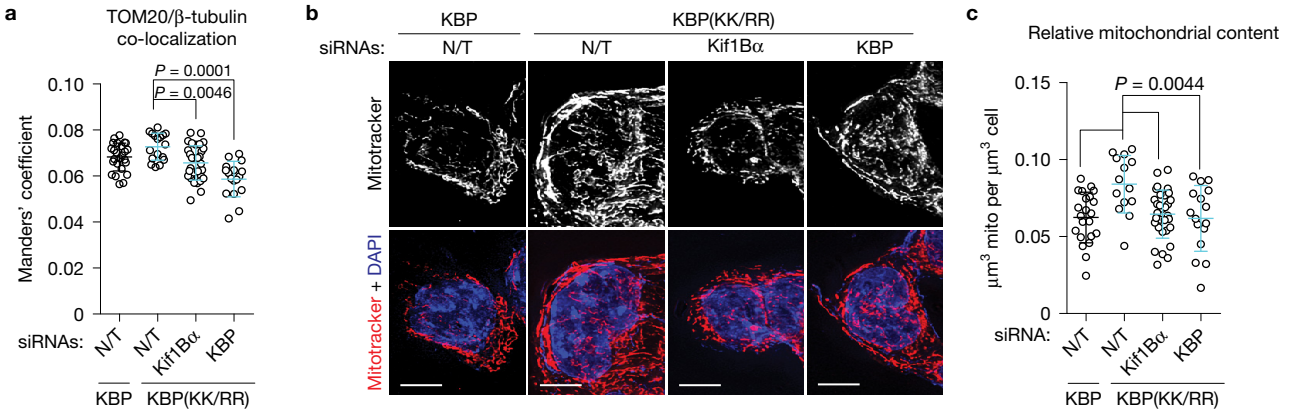

Figure 5 The mitochondrial biogenesis induced by KBP stabilization depends on Kif1Bα. (**a**) Following infection with lentiviruses expressing either HA-tagged WT mouse KBP or HA-tagged mouse KBP(KK/RR), mESCs were transfected with a non-targeting (N/T) siRNA or siRNAs to Kif1Bα or KBP, and immunostained for TOM20 and α-tubulin. Microtubule–mitochondria co-localization was detected by confocal microscopy and the Manders' overlap coefficient is shown. $n = 26$, 17, 28 and 17 cells (KBP+N/T siRNA, and KBP(KK/RR)+N/T, or Kif1Bα or KBP siRNA, respectively). P value was calculated by one-way ANOVA. Error bars indicate ± s.d. (**b**,**c**) Cells treated as in **a** were stained with Mitotracker and DAPI. 3D images were collected through widefield microscopy and reconstructed by 3D deconvolution. Panel **b** shows representative MIPs of the mitochondrial network of KBP- and KBP(KK/RR)-expressing mESCs, with or without depletion of Kif1Bα or KBP (scale bars, 15 μm). Panel **c** shows quantification of average mitochondrial content per μm^3. $n = 22$, 14, 31 and 16 cells (KBP+N/T siRNA, KBP(KK/RR)+N/T, or Kif1Bα or KBP siRNA, respectively). P value was calculated by one-way ANOVA. Error bars indicate ± s.d.

interaction between KBP and Fbxo15 in mESCs (Fig. 2d), suggesting that the activity of TDH and the consequent production of acetyl-CoA are a requirement for the recognition of KBP by Fbxo15. Importantly, Qc-1 treatment, Fbxo15 knockout, or knockdown of Fbxo15, GCN5L1 or TDH in mESCs did not activate the cell differentiation program, as shown by the unchanged levels of the pluripotency core factors Oct-3/4 and Sox2 (Figs 1b and 2a,b, and Supplementary Fig. 3a–d). Accordingly, expression of KBP(KK/RR) did not cause any major transcriptional changes (including transcription of pluripotency core factors), as detected by RNA-sequencing (Supplementary Fig. 4 and Supplementary Table 2).

Fbxo15 and TDH are transcriptionally downregulated when mESCs are induced to differentiate[9,23]. We confirmed that the reduction of Fbxo15 and TDH protein levels occurs rapidly following loss of pluripotency, with similar kinetics in cells induced to differentiate with either retinoic acid or neurobasal medium (Fig. 2a and Supplementary Fig. 3a and d). Moreover, under these differentiation conditions, the levels of KBP were similar to the levels observed when Fbxo15, GCN5L1 or TDH were depleted from self-renewing mESCs (Fig. 2a and Supplementary Fig. 3a and d). Collectively, our results show that the concerted activities of Fbxo15, GCN5L1 and TDH are required to keep KBP levels low during pluripotency, and suggest that the decrease in the levels of Fbxo15 and TDH at the onset of differentiation allows for the accumulation of KBP.

Failure to degrade KBP in mESCs enhances mitochondrial biogenesis in a Kif1Bα-dependent manner

Next, we investigated the biological significance of KBP degradation in self-renewing mESCs, by expressing either wild-type KBP or KBP(KK/RR) at near-to-physiologic levels (see Fig. 1d). KBP has been proposed to mediate mitochondrial transport and microtubule dynamics[14,16]. We found no difference in mitochondrial motility between mESCs expressing wild-type KBP or KBP(KK/RR) (Fig. 3a). Microtubules exert an active role in mitochondrial network remodelling[28], and the KBP–Kif1Bα complex has been reported to act as a bridge between microtubules and mitochondria[15]. Accordingly, using three-dimensional (3D) reconstructions, we observed that the expression of KBP(KK/RR) significantly enhanced the co-localization between mitochondria and β-tubulin (Fig. 3b). Similar results were obtained when Fbxo15 expression was depleted or TDH was briefly pharmacologically inhibited (Supplementary Fig. 5a,b).

Following induction of differentiation, mESCs undergo mitochondrial biogenesis. This is required to allow cells to adapt to the metabolic switch in favour of oxidative phosphorylation induced by differentiation[3,5,29]. We confirmed that mESCs expanded their mitochondrial content 24 h after the induction of differentiation (Supplementary Fig. 5c). This increase occurs before the induction of PGC-1α, a master regulator of mitochondrial biogenesis (Fig. 2a). Significantly, reconstructing 3D images by 3D deconvolution, we found that, compared with wild-type KBP, expression of KBP(KK/RR) in self-renewing mESCs induced a significant increase in the number of mitochondria per cell, the mitochondrial volume per cell, and the average volume of individual mitochondria (Fig. 3c–f). Moreover, mESCs expressing KBP(KK/RR) displayed an increase in mitochondrial DNA and specific mitochondrial proteins (that is, TOM20 and COX-IV) compared with mESCs expressing wild-type KBP (Fig. 3g,h). Similar results were obtained by knocking out Fbxo15 (Fig. 4a–c), inhibiting TDH in self-renewing mESCs (Fig. 4d–f), or silencing Fbxo15 (Supplementary Fig. 5d–g). The increase in mitochondrial content was dependent on KBP expression, as the knockdown of KBP reverted the effect obtained by silencing Fbxo15 (Supplementary Fig. 5d,e) or inhibiting TDH (Fig. 4d,e).

Importantly, Qc-1 treatment of mESCs stably transduced with wild-type KBP induced both an accumulation of exogenous KBP (Supplementary Fig. 6a) (in agreement with what is observed

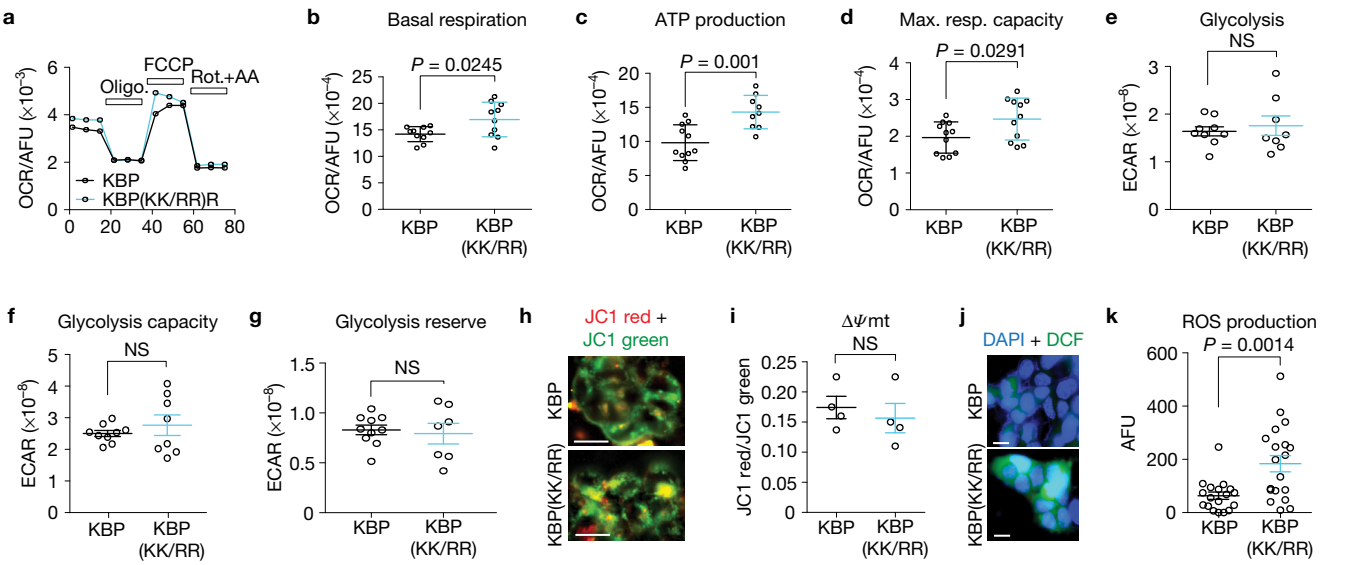

Figure 6 Effects of KBP accumulation on mitochondrial respiration. (**a**–**d**) mESCs infected with lentiviruses expressing either HA-tagged WT mouse KBP or HA-tagged mouse KBP(KK/RR) were analysed for their mitochondrial respiratory capacity. AFU, arbitrary fluorescence unit. Panel **a** shows cell representative kinetics of oxygen consumption rate (OCR). Oligo., oligomycin; Rot., rotenone; AA, antimycin A. Panel **b** compares cellular basal respiration. Panel **c** reports ATP synthase-dependent mitochondrial OCR. Panel **d** shows the maximal respiratory capacity. *P* values were calculated by unpaired *t*-test. Error bars, s.e.m.; $n=10$ independent cell culture dishes. (**e**–**g**) mESCs were infected with lentiviruses expressing either HA-tagged WT mouse KBP or HA-tagged mouse KBP(KK/RR). Cells underwent a real-time analysis of glycolysis through the measurement of the extracellular acidification rate (ECAR) after the induction of acute metabolic stress. *P* value was calculated by unpaired *t*-test. Error bars, s.e.m; $n=8$ independent cell culture dishes. NS, not significant. (**h**,**i**) mESCs were infected with lentiviruses expressing either HA-tagged WT mouse KBP or HA-tagged mouse KBP(KK/RR) and the $\Delta\psi$mt was measured using the ratiometric $\Delta\psi$mt-sensitive dye JC1. Panel **h** shows representative images. *P* value was calculated by unpaired *t*-test. Error bars, s.e.m.; $n=4$ independent cell culture dishes (see Supplementary Table 6). Scale bars, 15 μm. NS, not significant. (**j**,**k**) mESCs were infected with lentiviruses expressing either HA-tagged WT mouse KBP or HA-tagged mouse KBP(KK/RR) and analysed for ROS production using the peroxide-sensitive dye dichlorofluorescein (DCF). Panel **j** shows representative images. *P* value was calculated by unpaired *t*-test. Error bars, s.e.m. $n=18$ and 20 independent cell culture dishes (KBP and KBP(KK/RR), respectively). Scale bars, 20 μm.

with endogenous KBP (Supplementary Fig. 3b,c)) and an increase in mitochondrial number similar to what is observed in mESCs that were induced to differentiate (Supplementary Fig. 6b,c). In contrast, in mESCs expressing KBP(KK/RR), Qc-1 treatment failed to increase the already high levels of KBP(KK/RR) (Supplementary Fig. 6a). Moreover, KBP(KK/RR)-expressing mESCs displayed high mitochondrial content regardless of their Qc-1 treatment or differentiation status (Supplementary Fig. 6b,c).

The stabilization of KBP did not affect the rate of fission and fusion events (Supplementary Fig. 7), suggesting that the observed increase in mitochondrial mass is due to *de novo* biogenesis.

As KBP stabilization results in its enhanced interaction with Kif1Bα (Fig. 1d) and increased mitochondria–microtubule association (Fig. 3a and Supplementary Fig. 5a,b), we silenced Kif1Bα, which connects KBP to microtubules, in mESCs expressing KBP(KK/RR). Notably, depletion of Kif1Bα reversed the enhancement of mitochondria–microtubule co-localization (Fig. 5a) and the increased mitochondrial biogenesis induced by KBP(KK/RR) (Fig. 5b,c), showing that the effects of KBP on mitochondria depend on Kif1Bα.

KBP degradation preserves the fitness of mESCs

To evaluate the performance of mitochondria in KBP(KK/RR)-expressing mESCs, we measured critical cellular bioenergetic parameters. We found that the increase in mitochondrial mass was accompanied by an increase in respiration and ATP production, without affecting glycolysis (Fig. 6a–g). We also measured the differential membrane potential ($\Delta\psi$mt) at the mitochondria, and found that wild-type KBP and KBP(KK/RR)-expressing mESCs did not differ in $\Delta\psi$mt (Fig. 6h,i) and, therefore, had comparable individual mitochondrion activity. Taken together, these data show that KBP(KK/RR)-expressing mESCs perform increased mitochondrial respiration due to an overall higher mitochondrial mass and not a metabolic switch. Importantly, KBP stabilization promoted production of ROS (Fig. 6j,k).

On the basis of the last results, we assessed whether impairing the degradation of KBP affected cell growth rate. We found that KBP(KK/RR)-expressing mESCs proliferated significantly slower than wild-type KBP-expressing mESCs (Fig. 7a). The observation that Fbxo15 knockout and Fbxo15 silencing significantly reduced the proliferation of mESCs (Fig. 7b,c) corroborated our finding. This reduction in the growth rates of Fbxo15 is compatible with the observation that the average litter size of *Fbxo15*$^{-/-}$ mice is significantly smaller than that of *Fbxo15*$^{+/+}$ mice (Fig. 7d).

KBP accumulation is necessary for mitochondrial biogenesis during differentiation

Altogether, the experiments in Figs 3c–f, 4a,b,d,e and Supplementary Figs 5 and 6 demonstrate that the defects in KBP degradation in naive mESCs result in the acquisition of a mitochondrial content that is typically observed at the beginning of differentiation.

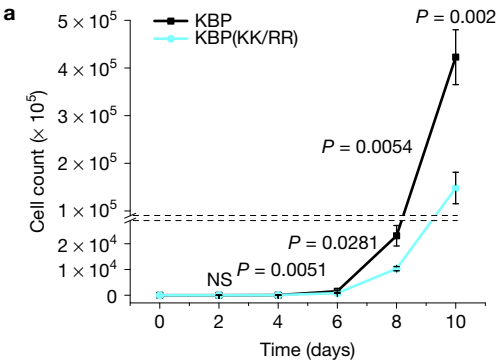

Time	KBP	KBP(KK/RR)
0	3.0×10^4	3.0×10^4
2	4.1×10^5	3.4×10^5
4	6.0×10^6	5.3×10^6
6	15.4×10^7	7.7×10^7
8	2.3×10^9	1.0×10^9
10	4.2×10^{10}	1.4×10^{10}

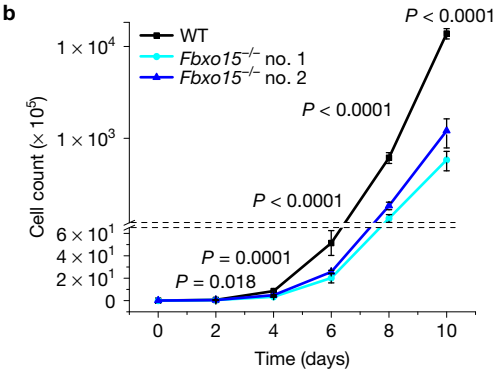

Time	WT	*Fbxo15*$^{-/-}$ no. 1	*Fbxo15*$^{-/-}$ no. 2
0	3.0×10^4	3.0×10^4	3.00×10^4
2	6.2×10^5	5.0×10^5	5.40×10^5
4	8.5×10^6	3.3×10^6	4.80×10^6
6	5.1×10^7	2.0×10^7	2.55×10^7
8	6.1×10^8	1.3×10^8	1.80×10^8
10	13.8×10^9	0.6×10^9	1.20×10^9

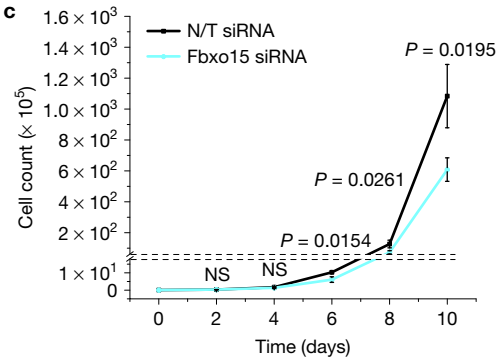

Time	N/T siRNA	Fbxo15 siRNA
0	3.0×10^4	3.0×10^4
2	3.0×10^5	3.1×10^5
4	1.7×10^6	1.3×10^6
6	1.0×10^7	0.6×10^7
8	1.2×10^8	0.7×10^8
10	1.0×10^{10}	0.6×10^9

d

	Fbxo15$^{+/+}$ × *Fbxo15*$^{+/+}$	*Fbxo15*$^{-/-}$ × *Fbxo15*$^{-/-}$
Average number of pups	7.43 ± 1.65	5.96 ± 1.96 *
Number of pregnancies	14	24
Total number of pups	104	143

Figure 7 *In vivo* and *in vitro* effects of KBP stabilization and loss of Fbxo15 on mESC growth. (**a**) mESCs were infected with lentiviruses expressing either HA-tagged WT mouse KBP or HA-tagged mouse KBP(KK/RR) and plated at a density of 3×10^4 cells per well. Every 48 h, cells were trypsinized, counted and re-plated at a 1:10 dilution. No changes in viability and cell death were detected in the two groups by Annexin-V/PI analysis (0.25% ± 0.127 for WT KBP and 0.29% ± 0.255 for KBP(KK/RR); $n=2$ biologically independent experiments (see Supplementary Table 6)). The right panel summarizes the average of each cell count. *P* value was calculated by unpaired *t*-test. Error bars indicate ± s.d. $n=3$ biologically independent experiments (see Supplementary Table 6). (**b**) WT mESCs and *Fbxo15*$^{-/-}$ mESCs (two different clones) were plated at a density of 3×10^4 cells per well. Every 48 h, cells were trypsinized, counted and re-plated at a 1:10 dilution. Cell counts were performed using a Vi-CELL, an automated cell counter that simultaneously assesses cell viability. No changes in viability were detected in the three groups. The right panel summarizes the average of each cell count. *P* value was calculated by one-way ANOVA. Error bars indicate ± s.d. $n=3$ biologically independent experiments (see Supplementary Table 6). (**c**) mESCs were transfected with either a non-targeting (N/T) siRNA or an siRNA against Fbxo15 and plated at a density of 3×10^4 cells per well. Every 48 h, cells were trypsinized, counted and re-plated at a 1:10 dilution with a further round of siRNA transfection. Cell counts were performed using a Vi-CELL, an automated cell counter that simultaneously assesses cell viability. No changes in viability were detected in the two groups. The right panel summarizes the average of each cell count. *P* value was calculated by unpaired *t*-test. Error bars indicate ± s.d. $n=3$ biologically independent experiments (see Supplementary Table 6). (**d**) *Fbxo15*$^{+/+}$ and *Fbxo15*$^{-/-}$ mice were mated and the average offspring per litter was compared. $n=14$ and 24 pregnancies. *, $P=0.0242$, calculated with unpaired *t*-test (see Supplementary Table 6). NS, not significant.

Conversely, when Fbxo15 and TDH were overexpressed in mESCs undergoing differentiation, a statistically significant reduction of mitochondrial content was observed (Fig. 8a,b). This result suggests that Fbxo15 and TDH are downregulated following the initiation of differentiation to allow the accumulation of KBP and the expansion of the mitochondrial network. To further substantiate

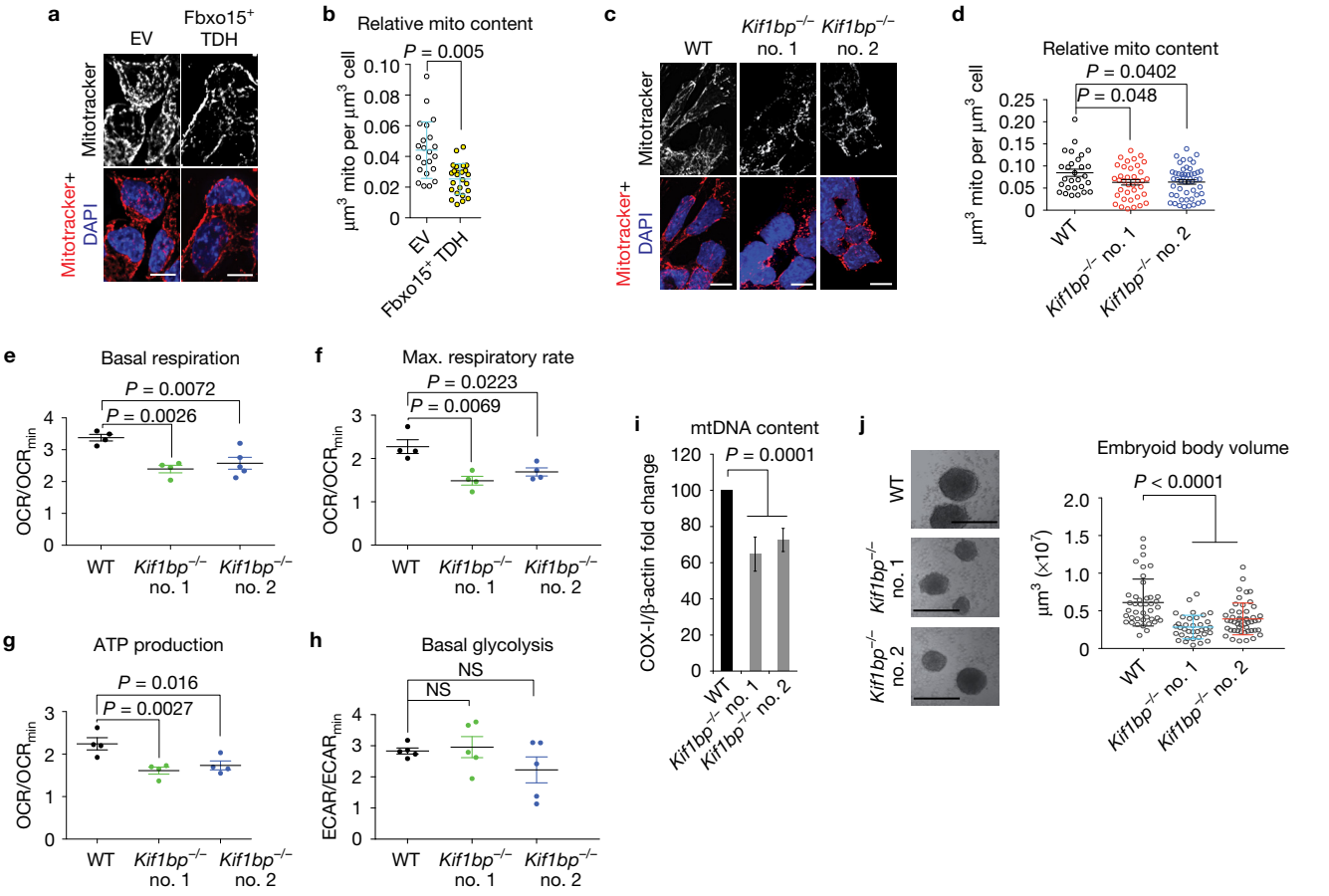

Figure 8 Ectopic expression of Fbxo15 and TDH reduces the mitochondrial content in differentiating mESCs, and *Kif1bp* knockout impairs mitochondrial biogenesis and differentiation. (**a**,**b**) mESCs were transfected with either empty (EV) or Fbxo15- and TDH-expressing vectors, and induced to differentiate for 24 h. Panel **a** shows the MIPs of representative cells (scale bars, 15 μm). Panel **b** shows the average mitochondrial content. $n = 22$ and 24 cells (EV and Fbxo15+TDH, respectively). This experiment was performed twice. *P* value was calculated by unpaired *t*-test. Error bars indicate ± s.d. (**c**,**d**) WT and *Kif1bp*$^{-/-}$ mESCs (two different clones) were induced to differentiate with retinoic acid for 48 h. Cells were stained with Mitotracker and DAPI prior to fixation and then analysed by confocal microscopy. Panel **c** shows the MIPs of representative cells (scale bars, 15 μm). Panel **d** shows the average mitochondrial content. $n = 28$, 38 and 52 cells (WT, *Kif1bp*$^{-/-}$ no. 1, and *Kif1bp*$^{-/-}$ no. 2, respectively). *P* value was calculated by one-way ANOVA. Error bars indicate ± s.d. (**e**–**h**) Cells treated as in **c** were analysed for their mitochondrial respiratory capacity. Panel **e** compares cellular basal respiration. Panel **f** shows the maximal respiratory capacity. Panel **g** reports ATP synthase-dependent mitochondrial OCR. Panel **h** shows glycolytic capacity. OCR_{min}, minimal detectable OCR; $ECAR_{min}$, minimal detectable ECAR. *P* value was calculated by one-way ANOVA. Scale bars, s.e.m.; $n = 4$ or 5 independent cell culture dishes (see Supplementary Table 6). NS, not significant. (**i**) Cells as in **c** were induced to generate embryoid bodies. After 4 days, total cellular DNA was extracted and mtDNA copy number was evaluated by qPCR normalized using β-actin DNA copy number. mtDNA amount in WT mESCs was set as 100 and the graph shows the fold change. *P* value was calculated by one-way ANOVA. Error bars indicate ± s.d. $n = 4$ independent cell culture dishes (see Supplementary Table 6). (**j**) Embryoid bodies were generated as in **i** and volume was calculated. The left panel shows representative images (scale bars, 400 μm). $n = 42$, 35 and 49 embryoid bodies (WT, *Kif1bp*$^{-/-}$ no. 1, and *Kif1bp*$^{-/-}$ no. 2, respectively). *P* value was calculated by one-way ANOVA. Error bars indicate ± s.d.

this hypothesis, we eliminated both alleles of *Kif1bp* (the gene encoding KBP) in mESCs employing a CRISPR/Cas9-dependent strategy (Supplementary Fig. 8a,b). We found that in 2 out 2 clones, the absence of KBP induced a defect in both respiration and differentiation. Specifically, we observed that, compared with wild-type cells, KBP-null cells induced to differentiate displayed reduced mitochondrial mass, mitochondrial DNA, oxygen consumption and ATP production, without a compensatory increase in basal glycolysis (Fig. 8c–i). Notably, the absence of KBP induced a reduction in the volume of embryoid bodies and a change in the transcriptional signature (Fig. 8j and Supplementary Tables 3 and 4), probably due to an energetic disadvantage.

DISCUSSION

In this study, we have described a regulatory network that controls mitochondrial biogenesis through the proteolysis of KBP in mESCs. Defects in KBP degradation do not affect the expression of the pluripotency core factors, supporting a model in which the observed effects on mitochondrial biogenesis are due to a mechanism that acts locally at the mitochondria, independently of transcriptional changes. Since stabilized KBP binds Kif1Bα and promotes the association of mitochondria to microtubules, we speculate that this association provides a microtubule track along which mitochondria grow. In addition, the motor activity of Kif1Bα may increase the mechanical forces applied to mitochondria, which, in turn, may promote the

growth of these organelles through a mechanism that is reminiscent of that acting at the level of the muscle fibre in which the application of force or mechanical tension is responsible for increasing the number of sarcomeres. In support of this proposed mechanism, Kif1Bα silencing reverts the phenotypes induced by the stabilization of KBP. A role of the microtubule network in mitochondrial biogenesis was previously proposed[30] and our findings integrate and expand those observations.

Importantly, we found that the mitochondrial-specific production of acetyl-CoA by TDH is required for GCN5L1 to acetylate KBP, which allows its recognition by Fbxo15 (see model in Supplementary Fig. 8c). In this context, mitochondrial outsourced acetyl-CoA, rather than being a mere substrate for protein acetylation, could be considered analogous to an intracellular messenger that is locally sensed by the GCN5L1–Fbxo15 machinery. In self-renewing naive mESCs, this machinery controls KBP levels and acts as a gatekeeper of the mitochondria steady state, thus, reducing ROS production and preserving the optimal fitness of mESCs. When naive mESCs are induced to differentiate, levels of Fbxo15 and TDH decrease, acetylation of KBP on Lys501 is inhibited, and KBP levels increase (Supplementary Fig. 8d).

In vivo, around the time of implantation, derivative cells of the inner cell mass—the embryonic counterpart of cultured naive mESCs—enter a so-called primed pluripotent state, which is characterized by profound transcriptional rearrangements that include the downregulation of Fbxo15 and TDH[26]. At this developmental stage, pluripotent cells display a more expanded mitochondrial network[31], in agreement with our model; yet, their oxidative phosphorylation is inhibited, due to a downregulation of key components of the respiratory chain[31,32].

Loss of *Fbxo15* in mice does not induce major defects (ref. 9 and http://www.mousephenotype.org/data/genes/MGI:1354755#section-associations). This could be due to compensatory events occurring in the $Fbxo15^{-/-}$ embryo and/or the fact that the time window of naive pluripotency in which Fbxo15 is expressed is very limited (~1 day)[33], and animals are fine once they have passed this bottleneck. This latter hypothesis is in agreement with the observed cell proliferation defects of $Fbxo15^{-/-}$ mESCs, as well as with the reduced litter size of $Fbxo15^{-/-}$ mice compared with $Fbxo15^{+/+}$ animals. Follow-up work might clarify whether and how loss of *Fbxo15* plays a role in early development.

In conclusion, we propose that KBP degradation is necessary to keep mitochondrial biogenesis in check during self-renewal. In contrast, the accumulation of KBP occurring after the induction of differentiation of mESCs is functional to their increase in mitochondrial mass, which allows proper differentiation. □

METHODS

Methods, including statements of data availability and any associated accession codes and references, are available in the online version of this paper.

Note: Supplementary Information is available in the online version of the paper

ACKNOWLEDGEMENTS

The authors thank C. Haynes, J. K. Pagan and T. Pozzan for critical reading of the manuscript; I. Aifantis (NYU School of Medicine, USA), R. Lammers (University of Tubingen, Germany), M. N. Sack (National Institutes of Health, USA) and F. Zhang (Massachusetts Institute of Technology, USA) for reagents. M.P. is grateful to T. M. Thor and T. B. Balduur for continuous support. V.D. is grateful to F. Catalanotti, G. Donato and A. Donato for continuous support. P.P. is grateful to C. d. Scrovegni for providing continuous support. This work was funded by grants from the National Institutes of Health (R37-CA076584, R01-GM057587 and R21-CA161108) and New York State Health Department (NYSTEM-N11G-255) to M.P.; the American-Italian Cancer Foundation and the National Institutes of Health (5T32CA009161-40) to V.D.; and The Italian Ministry of Health and the Italian Ministry of Education, University and Research (COFIN no. 20129JLHSY_002, FIRB no. RBAP11FXBC_002, and Futuro in Ricerca no. RBFR10EGVP_001), Telethon (GGP15219/B), the Italian Cystic Fibrosis Research Foundation (19/2014) and the Italian Association for Cancer Research (IG-18624) and local funds from the University of Ferrara and the Italian Ministry of Health to P.P. The authors also thank the NYU Genome Technology Center (partially funded by the Perlmutter Cancer Center Support Grant P30CA016087) for expert library preparation and sequencing for RNA-seq, and the NYU Applied Bioinformatics Laboratories for providing bioinformatics support and helping with the analysis and interpretation of the RNA-seq data using computing resources at the NYU High Performance Computing Facility. A.S., L.F. and M.P.W. are supported by the Stowers Institute for Medical Research. M.P. is an Investigator with the Howard Hughes Medical Institute.

AUTHOR CONTRIBUTIONS

V.D. conceived the project, planned and performed most experiments, and co-wrote the manuscript. M.P. directed and coordinated the study, oversaw the results, and co-wrote the manuscript. M.B. and P.P. performed analyses of mitochondrial morphology and physiology. D.Simoneschi generated the CRISPR knockout mESC clones and helped with biochemical experiments and with RNA-seq data analysis. D.Sartini helped with some biochemical experiments. Y.K. performed the $Fbxo15^{+/+}$ and $Fbxo15^{-/-}$ mouse breeding. M.S. provided reagents and advice. A.S., L.F. and M.P.W. performed the mass spectrometry analyses of the purifications performed by V.D. All authors discussed the results and commented on the manuscript.

COMPETING FINANCIAL INTERESTS

The authors declare no competing financial interests.

Published online at http://dx.doi.org/10.1038/ncb3491

1. Dyall, S. D., Brown, M. T. & Johnson, P. J. Ancient invasions: from endosymbionts to organelles. *Science* **304,** 253–257 (2004).
2. Giorgi, C. *et al.* Mitochondrial Ca^{2+} and apoptosis. *Cell Calcium* **52,** 36–43 (2012).
3. Xu, X. *et al.* Mitochondrial regulation in pluripotent stem cells. *Cell Metab.* **18,** 325–332 (2013).
4. Rafalski, V. A., Mancini, E. & Brunet, A. Energy metabolism and energy-sensing pathways in mammalian embryonic and adult stem cell fate. *J. Cell Sci.* **125,** 5597–5608 (2012).
5. Rehman, J. Empowering self-renewal and differentiation: the role of mitochondria in stem cells. *J. Mol. Med.* **88,** 981–986 (2010).
6. Wanet, A., Arnould, T., Najimi, M. & Renard, P. Connecting mitochondria, metabolism, and stem cell fate. *Stem Cells Dev.* **24,** 1957–1971 (2015).
7. Lin, J. *et al.* Transcriptional co-activator PGC-1α drives the formation of slow-twitch muscle fibres. *Nature* **418,** 797–801 (2002).
8. Spiegelman, B. M. Transcriptional control of energy homeostasis through the PGC1 coactivators. *Novartis Found. Symp.* **286,** 3–6 (2007).
9. Tokuzawa, Y. *et al.* Fbx15 is a novel target of Oct3/4 but is dispensable for embryonic stem cell self-renewal and mouse development. *Mol. Cell. Biol.* **23,** 2699–2708 (2003).
10. Takahashi, K. & Yamanaka, S. Induction of pluripotent stem cells from mouse embryonic and adult fibroblast cultures by defined factors. *Cell* **126,** 663–676 (2006).
11. Skaar, J. R., Pagan, J. K. & Pagano, M. Mechanisms and function of substrate recruitment by F-box proteins. *Nat. Rev. Mol. Cell Biol.* **14,** 369–381 (2013).
12. Chen, B. B. *et al.* E3 ligase subunit Fbxo15 and PINK1 kinase regulate cardiolipin synthase 1 stability and mitochondrial function in pneumonia. *Cell Rep.* **7,** 476–487 (2014).
13. Brooks, A. S. *et al.* Homozygous nonsense mutations in KIAA1279 are associated with malformations of the central and enteric nervous systems. *Am. J. Hum. Genet.* **77,** 120–126 (2005).
14. Lyons, D. A., Naylor, S. G., Mercurio, S., Dominguez, C. & Talbot, W. S. KBP is essential for axonal structure, outgrowth and maintenance in zebrafish, providing insight into the cellular basis of Goldberg-Shprintzen syndrome. *Development* **135,** 599–608 (2008).
15. Hirokawa, N., Niwa, S. & Tanaka, Y. Molecular motors in neurons: transport mechanisms and roles in brain function, development, and disease. *Neuron* **68,** 610–638 (2010).

16. Wozniak, M. J., Melzer, M., Dorner, C., Haring, H. U. & Lammers, R. The novel protein KBP regulates mitochondria localization by interaction with a kinesin-like protein. *BMC Cell Biol.* **6,** 35 (2005).
17. Kevenaar, J. T. *et al.* Kinesin-binding protein controls microtubule dynamics and cargo trafficking by regulating kinesin motor activity. *Curr. Biol.* **26,** 849–861 (2016).
18. Drerup, C. M., Lusk, S. & Nechiporuk, A. Kif1B interacts with KBP to promote axon elongation by localizing a microtubule regulator to growth cones. *J. Neurosci.* **36,** 7014–7026 (2016).
19. Still, A. J. *et al.* Quantification of mitochondrial acetylation dynamics highlights prominent sites of metabolic regulation. *J. Biol. Chem.* **288,** 26209–26219 (2013).
20. Scott, I., Webster, B. R., Li, J. H. & Sack, M. N. Identification of a molecular component of the mitochondrial acetyltransferase programme: a novel role for GCN5L1. *Biochem J.* **443,** 655–661 (2012).
21. Webster, B. R. *et al.* Restricted mitochondrial protein acetylation initiates mitochondrial autophagy. *J. Cell Sci.* **126,** 4843–4849 (2013).
22. Scott, I. *et al.* GCN5-like protein 1 (GCN5L1) controls mitochondrial content through coordinated regulation of mitochondrial biogenesis and mitophagy. *J. Biol. Chem.* **289,** 2864–2872 (2014).
23. Wang, J. *et al.* Dependence of mouse embryonic stem cells on threonine catabolism. *Science* **325,** 435–439 (2009).
24. Shyh-Chang, N. *et al.* Influence of threonine metabolism on S-adenosylmethionine and histone methylation. *Science* **339,** 222–226 (2013).
25. Kim, J., Chu, J., Shen, X., Wang, J. & Orkin, S. H. An extended transcriptional network for pluripotency of embryonic stem cells. *Cell* **132,** 1049–1061 (2008).
26. Buecker, C. *et al.* Reorganization of enhancer patterns in transition from naive to primed pluripotency. *Cell Stem Cell* **14,** 838–853 (2014).
27. Alexander, P. B., Wang, J. & McKnight, S. L. Targeted killing of a mammalian cell based upon its specialized metabolic state. *Proc. Natl Acad. Sci. USA* **108,** 15828–15833 (2011).
28. Friedman, J. R., Webster, B. M., Mastronarde, D. N., Verhey, K. J. & Voeltz, G. K. ER sliding dynamics and ER-mitochondrial contacts occur on acetylated microtubules. *J. Cell Biol.* **190,** 363–375 (2010).
29. Prowse, A. B. *et al.* Analysis of mitochondrial function and localisation during human embryonic stem cell differentiation *in vitro*. *PLoS ONE* **7,** e52214 (2012).
30. Karbowski, M. *et al.* Opposite effects of microtubule-stabilizing and microtubule-destabilizing drugs on biogenesis of mitochondria in mammalian cells. *J. Cell Sci.* **114,** 281–291 (2001).
31. Zhou, W. *et al.* HIF1α induced switch from bivalent to exclusively glycolytic metabolism during ESC-to-EpiSC/hESC transition. *EMBO J.* **31,** 2103–2116 (2012).
32. Carbognin, E., Betto, R. M., Soriano, M. E., Smith, A. G. & Martello, G. Stat3 promotes mitochondrial transcription and oxidative respiration during maintenance and induction of naive pluripotency. *EMBO J.* **35,** 618–634 (2016).
33. Pauklin, S., Pedersen, R. A. & Vallier, L. Mouse pluripotent stem cells at a glance. *J. Cell Sci.* **124,** 3727–3732 (2011).

DOI: 10.1038/ncb3491

METHODS

Cell culture. mESCs were kindly provided by I. Aifantis and maintained on gelatin-coated tissue culture plates with LIF/2i as described in ref. 34. ESCs were trypsinized and passaged every 48 h and periodically checked for the expression of pluripotency markers. mESCs differentiation was induced either by LIF/2i withdrawal and supplementation with 10 μM retinoic acid on gelatin-coated plates, or by seeding cells on non-adherent Petri dishes as in ref. 34. Where indicated, Qc-1 was administered at the concentration of 10 μM for 12 h. HEK293T cells were maintained in Dulbecco's modified Eagle's medium containing 10% fetal bovine serum. HEK293T cells were not authenticated, as they were not used in experiments designed for the functional characterization of KBP degradation. mESCs were not authenticated. Cells were periodically screened for *Mycoplasma* contamination. No cell lines used in this study were found in the database of commonly misidentified cell lines that is maintained by ICLAC and NCBI Biosample.

Transient transfections. siRNA duplexes (see Supplementary Table 5 for sequence details) were transfected into mESCs using RNAiMAX reagent (Life Technologies) according to the manufacturer's instructions. To achieve satisfactory RNAi-mediated depletion, siRNA duplexes were transfected over 2 or 3 rounds. Plasmids were transfected into mESCs using Lipofectamine 3000 (Life Technologies) according to the manufacturer's instructions. HEK293T cells were always transduced with vectors expressing human gene sequences, while mESCs were transfected with their mouse counterparts. HEK293T cells were transfected using the calcium phosphate method, as described previously[35].

Purification, MudPIT and PTM analyses. HEK293T cells were transfected with constructs encoding Strep-FLAG-tagged human Fbxo15, Strep-FLAG-tagged human Fbxo21, or Strep-FLAG-tagged human KBP(K504G) (the last one at the C terminus). Forty-eight hours after transfection, cells were collected and lysed in lysis buffer (50 mM Tris-HCl pH 7.5, 150 mM NaCl, 1 mM EDTA, 50 mM NaF, 0.5% NP-40, plus protease and phosphatase inhibitors). Proteins were immunopurified with Streptavidin beads (IBA) and, after extensive washing, eluted by competition with biotin. The eluate was then subjected to a second immunopurification with anti-FLAG M2 agarose beads (Sigma), prior to elution by competition with a 3x-FLAG peptide (Sigma). The final eluate was then precipitated with TCA. TCA-precipitated proteins were urea-denatured, reduced, alkylated and digested with endoproteinase Lys-C (Roche) and modified trypsin (Roche), as described in refs 36,37. Peptide mixtures were loaded onto 100 μm fused silica microcapillary columns packed with 5-μm C_{18} reverse phase (Aqua, Phenomenex), strong cation exchange particles (Partisphere SCX, Whatman)[38]. Loaded microcapillary columns were placed in-line with a Quaternary Agilent 1100 series HPLC pump and a LTQ linear ion trap mass spectrometer equipped with a nano-LC electrospray ionization source (ThermoFinnigan). Fully automated 10-step MudPIT runs were carried out on the electrosprayed peptides, as described in ref. 37. Tandem mass (MS/MS) spectra were interpreted using SEQUEST[39] against a database of 61,430 sequences, consisting of 30,552 human proteins (downloaded from NCBI on 4 March 2008), 177 usual contaminants and, to estimate false discovery rates, 30,712 randomized amino acid sequences derived from each non-redundant protein entry. Peptide/spectrum matches were sorted and selected using DTASelect[40] with the following criteria set: spectra/peptide matches were retained only if they had a DeltCn of at least 0.08 and a minimum XCorr of 1.8 for singly, 2.0 for doubly, and 3.0 for triply charged spectra. In addition, peptides had to be fully tryptic and at least 7 amino acids long. Combining all runs, proteins had to be detected by at least 2 such peptides, or 1 peptide with 2 independent spectra. Under these criteria the final FDRs at the protein and spectral levels were 1.6% and 0.13% ± 0.05, respectively. Peptide hits from multiple runs were compared using CONTRAST[40]. To estimate relative protein levels, normalized spectral abundance factors were calculated for each detected protein, as described in refs 37,41,42.

Biochemical methods. Extract preparation, immunoprecipitation, and immunoblotting have been previously described[43,44].

CRISPR genome editing. To generate *Kif1bp* and *Fbxo15* knockout mESCs, optimal gRNA target sequences closest to the genomic target sites were designed using the Benchling CRISPR Genome Engineering tool. *Kif1b* and Fbxo15 gRNA target sequences (see Supplementary Table 5) were cloned into pSpCas9(BB)-2A-GFP (PX458), a gift from F. Zhang (Addgene plasmid no. 48138)[45]. mESCs were seeded into 10 cm dishes at a ∼70% confluency, and transfected with 5 μg of the appropriate gRNA-containing PX458 plasmid, using Lipofectamine 3000 (Life Technologies). The transfection was performed according to the manufacturer's recommended protocol, using a 2:1 ratio of Lipofectamine/DNA. Two days after transfection, GFP-positive cells were sorted using the Beckman Coulter MoFlo XDP cell sorter (100 μm nozzle), and 15,000 cells were plated on a 15 cm dish. Eight to ten days later, single mESC clones were picked, trypsinized in 0.25% trypsin–EDTA for 5 min, and plated into individual wells of a 96-well plate for genotyping. Genomic DNA was collected using QuickExtract (Epicentre). Genotyping PCRs were performed with MangoTaq DNA Polymerase (Bioline), using primers surrounding the genomic target site. The resulting PCR products were purified and sequenced to determine the presence of an insertion or deletion event. To further validate the mutational status of candidate clones, the PCR products were subjected to TOPO-TA Cloning (Invitrogen), and sequenced to distinguish the amplified products of distinct alleles. Fifty bacterial colonies for each TOPO-TA cloning reaction were sequenced and aligned to the corresponding wild-type template in Benchling. Clones positive to insertion or deletion events were validated also by western blot.

Plasmids. Mouse KBP cDNA was amplified by PCR using a cDNA library generated from mESCs and then subcloned into pLenti-III-UbC (ABM). Mouse Fbxo15 and TDH were amplified by PCR using a cDNA library generated from mESCs and then subcloned into pHAGE2-EF1α[46]. Human Fbxo15, Fbxo21 and KBP cDNAs were amplified by PCR using a cDNA library generated from HEK293T cells. cDNAs were then subcloned into pcDNA 3.1 (Life Technologies). A plasmid expressing a mitochondrial-targeted GFP (mtGFP) under the MSCV promoter was purchased from ABM. Human and mouse KBP mutants were generated by either using the QuikChange Site-directed Mutagenesis kit (Stratagene) or by standard PCR procedures. All cDNAs were sequenced.

Stable infections. Lentiviruses were generated in HEK293T cells and concentrated as in ref. 46. Infections were carried as in ref. 47. Twenty-four hours after the infection, mESCs were selected with puromycin (1.5 μg ml^{-1}).

Antibodies. The anti-acetyl-KBP antibody was generated by immunizing rabbits with the peptide C-DSHIVKacKINNLNKSALKYYQLFLDSL after its conjugation with KLH. The following rabbit polyclonal antibodies were used: Fbxo15 (M-291; Santa Cruz Biotechnology; 1:500 dilution), KBP (kindly provided by R. Lammers, Tubingen, Germany; 1:5,000 dilution), Skp1 (H-163; Santa Cruz Biotechnology; 1:1,000 dilution), Oct-4 (no. PA5-27438, Thermo Fisher; 1:2,000 dilution), Sox2 (no. 48-1400, Thermo Fisher; 1:2,000 dilution), GCN5L1 (kindly provided by M. Sack, NIH; 1:1,000 dilution), PGC-1α (ST1204, Calbiochem; 1:1,000), caspase-3 (no. 9662, Cell Signaling Technologies; 1:1,000 dilution), NRF-2 (no. 12721, Cell Signaling Technologies; 1:1,000 dilution), PARP-1 (no. 9542, Cell Signaling Technologies; 1:1,000 dilution), HA (A190-108A, Bethyl; 1:5000 dilution) and FLAG (Sigma; 1:5,000 dilution). The following mouse monoclonal antibodies were used: TOM20 (no. 612278, BD; 1:2,000 dilution), α-tubulin (T5168; Sigma; 1:5,000 dilution), and COX-IV (4D11-B3-E8, Cell Signaling Technologies; 1:2,000 dilution). The following goat polyclonal antibodies were used: TDH (D-14; Santa Cruz Biotechnology; 1:1,000 dilution) and Kif1Bα (L-20; Santa Cruz Biotechnology; 1:1,000 dilution).

Immunofluorescence microscopy. For indirect immunofluorescence staining, mESCs were grown on StemXVivo matrix (RD Systems)-coated glass coverslips and then fixed with 4% paraformaldehyde for 10 min at room temperature. The cells were permeabilized with PBS/0.05% Triton X-100 for 10 min and blocked for 1 h in PBS/0.05% Triton X-100 containing 3% BSA prior to incubation with primary antibodies. Secondary antibodies were Alexa Fluor conjugated (Life Technologies). DAPI was used to counterstain DNA. Slides were mounted with ProLong Gold Antifade Mountant (Life Technologies). MitoTracker Red (Life Technologies) was incubated 30 min prior to fixation. Images were acquired at the Nyquist rate in x, y and z axes by an LSM 800 equipped with Zen software (Zeiss), or by a motorized custom epifluorescence microscope (Crisel Instruments). Three-dimensional co-localizations between mitochondria and microtubules were quantified according to the Manders' method using a custom-made Fiji macro as in ref. 48. To evaluate the extent of spontaneous mitophagy, cells were incubated with Mitotracker (Life Technologies) for 30′ in growth medium, washed in PBS and incubated with Lysotracker (Life Technologies) for 30′ in PBS +15% serum. Live cells were scanned with the Cytation 5 plate reader (Biotek). Co-localization coefficients were calculated in ImageJ using the JACoP plug-in.

Apoptosis assay. Annexin-V/PI staining was performed as previously described[49]. Two-dimensional flow cytometry was performed to detect Alexa-488-conjugated Annexin-V and PI using a LSRII flow cytometer (BD Biosciences) and FlowJo software (Tree Star).

Analysis of mitochondrial morphology. Three-dimensional images were reconstructed by 3D deconvolution using experimentally measured PSF and

the 3D iterative deconvolution plug-in for Fiji (available at: http://fiji.sc/Iterative_Deconvolve_3D). After reconstruction, cells were manually demarcated using the β-tubulin signal, which defines the cytosol limit. For each cell, mitochondria and nuclei were segmented automatically using the moment algorithm. Then object amount and size were obtained using the 3D object counter plug-in for Fiji (available at: http://fiji.sc/3D_Objects_Counter).

Quantification of mitochondrial DNA content. Total DNA was extracted from cells using the DNeasy Blood and Tissue Kit (Qiagen) following the manufacturer's instruction and used as the template for qPCR, using primers for COX-I (to assess the copies of mtDNA) and β-actin (to normalize the mtDNA content per cell) (see Supplementary Table 5 for primer sequences). The reaction was performed with a Roche480 thermal cycler, by using the Absolute Blue QPCR SYBR Green Mix (Thermo Scientific).

Mitochondrial tracking and mitochondrial dynamics analyses. mESCs were stained with Mitotracker Red according to the manufacturer's instructions, and then imaged with a Nikon Swept Field confocal equipped with CFI Plan Apo VC60XH objective (n.a. 1.4) and an Andor DU885 EM-CCD camera. Coverslips were placed in a chamber with controlled temperature, CO_2 and humidity; *z*-stacks were acquired by 73 planes with 0.3 µm distance, to allow acquisition of the whole cell. Images were acquired every 3 s for a total of 30 s. Mitochondrial movement was tracked through the Imaris software (Bitplane). Out of the total amount of mitochondria, the proportion of moving mitochondria was calculated. To assess the occurrence of events of mitochondrial fission and fusion, we applied an algorithm to detect a fusion event as an increase in the object volume larger than the smallest object detectable; inversely, a fission event was considered as a reduction in object volume larger than the smallest object detectable.

XF bioenergetic analysis. OCRs in mESCs were measured using the Seahorse XF96 bioanalyzer (Seahorse Biosciences) according to the manufacturer's protocols. Cells were seeded in an XF96 microplate at a density of 15,000 cells per well and allowed to attach. The following day or 48 h after the induction of differentiation, the medium was exchanged, where indicated, with 175 µl unbuffered XF assay media at pH 7.4 (Seahorse Biosciences) supplemented with 5.5 mM glucose (Sigma), 1 mM sodium pyruvate and 1 mM glutamine, or with 175 µl unbuffered XF assay media at pH 7.4 (Seahorse Biosciences) without glucose, sodium pyruvate or glutamine. Then, the microplate was placed in a 37 °C non-CO_2 incubator for 60 min. Respiration was measured in four blocks of three for 3 min each. The first block measured the basal respiration rate. Next, 1 µm oligomycin (Seahorse Biosciences) was added to inhibit complex V, and the second block was measured. Then, 1 µm FCCP (Seahorse Biosciences) was added to uncouple respiration and the third block was measured. Finally, 1 µm antimycin A (Seahorse Biosciences) and 1 µm rotenone (Seahorse Biosciences) were added to inhibit complex III and the last measurements were performed. Immediately after finishing the measurements, the cells were washed with PBS, fixed in 4% paraformaldehyde and stained with 1 µM DAPI. After staining, the plate was scanned on an automated Olympus Scan workstation and total DAPI content measured. An empty well was used as a background reference. For each well, the DAPI content (subtracted of the background) was used to normalize OCR values on cell content. Glycolysis capacity and reserve were measured in real-time with the Seahorse Bioanalyzer using the XF Glycolysis Stress Test Kit (Seahorse Biosciences), according to the manufacturer's recommendations. Briefly, cells were seeded in an XF96 microplate at a density of 15,000 cells per well and allowed to attach. The following day, the extracellular acidification rate was measured after triggering acute stress with the kit buffers.

Intracellular ROS measurement. mESCs infected with lentiviruses expressing wild-type KBP and KBP(KK/RR) were seeded in a 4-chamber 35 mm glass-bottom Petri dish (Cellvis) coated with 0.1% gelatin 24 h before the experiment. Then, the cells were stained with 1 µM 2′-7′dichlorodihydrofluorescein diacetate (H_2DCFDA, ThermoFisher) supplemented with 1 µM Hoechst and 0.02% Pluronic acid (Sigma-Aldrich) in Krebs ringer buffer supplemented with 1 g l^{-1} glucose and 1 mM $CaCl_2$ (complete KRB) for 30 min at 37 °C. After staining, the cells were washed with complete KRB and then measurements were acquired with an automated Olympus Scan workstation (Olympus). Fluorescence intensity in the FITC channel was measured for each cluster of cells.

Measurement of mitochondrial membrane potential. mESCs infected with lentiviruses expressing wild-type KBP and KBP(KK/RR) were seeded in a 4-chamber 35 mm glass-bottom Petri dish (Cellvis) coated with 0.1% gelatin 24 h before the experiment. Then, the cells were stained with JC1 (ThermoFisher) 0.2 µM in complete KRB for 30 min at 37 °C. After staining, the cells were washed with complete KRB and then measurements were acquired with an automated Olympus Scan workstation (Olympus). Integrated fluorescence intensities in the FITC and rhodamine channels were measured for each cluster of cells. The ratio between rhodamine and FITC channel intensity was used as an index of mitochondrial membrane potential extent.

RNA extraction and next-generation sequencing analysis. Libraries for RNA-seq were prepared according to the manufacturer's instructions (Illumina). Briefly, total RNA was extracted from cultured cells using the RNeasy Plus Mini Kit (QIAGEN). Poly(A) RNA was isolated using Dynabeads Oligo(dT)25 (Invitrogen) and used as input for library construction utilizing the dUTP method as described previously[50]. Barcodes were used for sample multiplexing. RNA libraries were sequenced on an Illumina HiSeq. RNA-seq data were mapped to mm10 (Genome Reference Consortium GRCm38) with Bowtie using parameters -v2 -m40. Sequence reads were assigned to genes using DEGseq (R package) and the ENSEMBL annotation. Differential gene expression was normalized using DESeq2 (R package) and the resulting values were used to generate an MA plot (that is, a Bland–Altman plot of $\log_2$ fold changes versus the mean of normalized counts).

Mice. Fbxo15$^{-/-}$ mice were originally generated by the Yamanaka laboratory (Kyoto University). Fbxo15$^{+/+}$ and Fbxo15$^{-/-}$ embryos were obtained from RIKEN BRC and backcrossed into a C57BL6 background for 5–6 generations. Both male and female mice in fertile age were used for breeding. For breeding experiments, randomization was not applicable and the operator was not blinded. All animal experiments were performed in accordance with protocols approved by the Tokushima University Institutional Animal Care and Use Committee.

Statistics and reproducibility. All data were collected and analysed by Prism 6 (Graphpad). Sample sizes and reproducibility for each figure are denoted in the figure legends. Unless otherwise noted, data are representative of at least three biologically independent experiments. For mouse experiments, no statistical method was used to predetermine sample size. Furthermore, the experiments were not randomized and the investigators were not blinded to allocation during experiments and outcome assessment. Two-group data sets were analysed by Student's unpaired *t*-test. For three- or four-group analysis, one-way or two-way ANOVA was used. All graphs show mean values. Error bars indicate ± s.d. or s.e.m., as indicated in the figure legends. Raw data from independent replicate experiments with $n < 5$ can be found in the Statistics Source Data file (Supplementary Table 6).

Data availability. The next-generation sequencing data that support the findings of this study in Supplementary Fig. 4 and in Supplementary Tables 2–4 have been deposited in the Gene Expression Omnibus (GEO) database under the accession code GSE84861. The MudPIT data that support the findings of this study have been provided in Supplementary Table 1. Statistics source data have been provided as Supplementary Table 6 and include data from Figs 3g, 4c,f, 6i, 7a–d and 8e–g,i and Supplementary Fig. 5f. All other data supporting the findings of this study are available from the corresponding author on reasonable request.

34. Narendra, V. *et al.* CTCF establishes discrete functional chromatin domains at the Hox clusters during differentiation. *Science* **347,** 1017–1021 (2015).
35. Young, L. M. *et al.* TIMELESS forms a complex with PARP1 distinct from its complex with TIPIN and plays a role in the DNA damage response. *Cell Rep.* **13,** 451–459 (2015).
36. Washburn, M. P., Wolters, D. & Yates, J. R. III Large-scale analysis of the yeast proteome by multidimensional protein identification technology. *Nat. Biotechnol.* **19,** 242–247 (2001).
37. Florens, L. *et al.* Analyzing chromatin remodeling complexes using shotgun proteomics and normalized spectral abundance factors. *Methods* **40,** 303–311 (2006).
38. MacCoss, M. J. *et al.* Shotgun identification of protein modifications from protein complexes and lens tissue. *Proc. Natl Acad. Sci. USA* **99,** 7900–7905 (2002).
39. Eng, J. K., McCormack, A. L. & Yates, J. R. An approach to correlate tandem mass spectral data of peptides with amino acid sequences in a protein database. *J. Am. Soc. Mass Spectrom.* **5,** 976–989 (1994).
40. Tabb, D. L., McDonald, W. H. & Yates, J. R. III DTASelect and Contrast: tools for assembling and comparing protein identifications from shotgun proteomics. *J. Proteome Res.* **1,** 21–26 (2002).
41. Paoletti, A. C. *et al.* Quantitative proteomic analysis of distinct mammalian Mediator complexes using normalized spectral abundance factors. *Proc. Natl Acad. Sci. USA* **103,** 18928–18933 (2006).
42. Zybailov, B. *et al.* Statistical analysis of membrane proteome expression changes in *Saccharomyces cerevisiae*. *J. Proteome Res.* **5,** 2339–2347 (2006).
43. D'Angiolella, V. *et al.* Cyclin F-mediated degradation of ribonucleotide reductase M2 controls genome integrity and DNA repair. *Cell* **149,** 1023–1034 (2012).
44. Kuchay, S. *et al.* FBXL2- and PTPL1-mediated degradation of p110-free p85β regulatory subunit controls the PI(3)K signalling cascade. *Nat. Cell Biol.* **15,** 472–480 (2013).

DOI: 10.1038/ncb3491

45. Ran, F. A. *et al*. Genome engineering using the CRISPR-Cas9 system. *Nat. Protoc.* **8,** 2281–2308 (2013).
46. Sommer, C. A. *et al*. Induced pluripotent stem cell generation using a single lentiviral stem cell cassette. *Stem Cells* **27,** 543–549 (2009).
47. Pagan, J. K. *et al*. Degradation of Cep68 and PCNT cleavage mediate Cep215 removal from the PCM to allow centriole separation, disengagement and licensing. *Nat. Cell Biol.* **17,** 31–43 (2015).
48. Giorgi, C. *et al*. p53 at the endoplasmic reticulum regulates apoptosis in a Ca^{2+}-dependent manner. *Proc. Natl Acad. Sci. USA* **112,** 1779–1784 (2015).
49. Dankert, J. F. *et al*. Cyclin F-mediated degradation of SLBP limits H2A.X accumulation and apoptosis upon genotoxic stress in G2. *Mol. Cell* **64,** 507–519 (2016).
50. Parkhomchuk, D. *et al*. Transcriptome analysis by strand-specific sequencing of complementary DNA. *Nucleic Acids Res.* **37,** e123 (2009).

nature cell biology

DOI: 10.1038/ncb3491

In the format provided by the authors and unedited.

a

Protein	dNSAF	Protein	dNSAF
Fbxo15	0.04721	Fbxo21	0.031288
Skp1	0.07519	Skp1	0.1498
Cul1	0.01805	Cul1	0.002008
KBP	0.000149	KBP	0

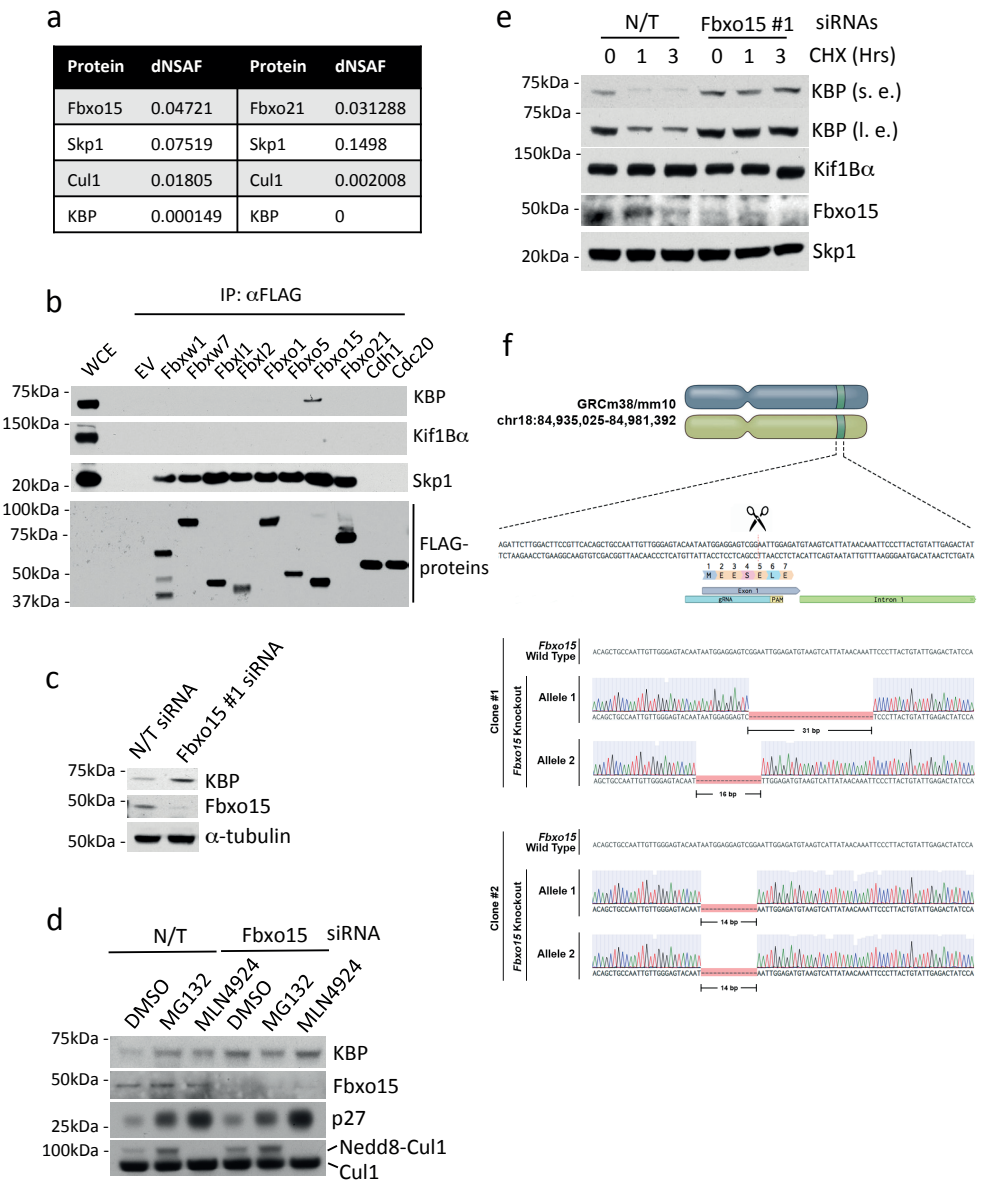

Supplementary Figure 1 Multidimensional Protein Identification Technology analysis of the Fbxo15 complex and its validation, and generation of *Fbxo15*$^{-/-}$ mESCs by CRISPR Genome Editing. a. HEK293T cells were transfected with either Strep-FLAG-tagged human Fbxo15 or Strep-FLAG-tagged human Fbxo21 (the latter used as control). The table shows the mass spectrometry analysis of the two immunopurifications, listing normalized spectral abundance factors (NSAFs) for the indicated proteins. The complete list of Fbxo15 interactors is reported in Supplementary Table 1. This experiment was performed twice. b. HEK293T cells were transfected with an empty vector (EV) or constructs for the indicated human proteins. Whole cell extracts (WCE) were immunoprecipitated (IP) with anti-FLAG resin, and immunocomplexes were immunoblotted as indicated. **c.** mESCs were transfected with either an siRNA to Fbxo15 (oligo #1) or a nontargeting (N/T) siRNA. Protein extracts were then immunoblotted for the indicated proteins. d. mESCs were transfected with either a nontargeting (N/T) siRNA or siRNA to Fbxo15 and treated for 4 hours with MG132, MLN4924, or DMSO. Cells were then collected and lysed for immunoblotting as indicated. The Nedd8-activating enzyme inhibitor MLN4924 blocks the neddylation of Cul1, which is required for the SCF activity. p27, an established substrate of the proteasome and the F-box protein Skp2, is used as positive control for MG132 and MLN4924, and as a negative control for Fbxo15 silencing. e. mESCs were transfected with either an siRNA to Fbxo15 (oligo #1) or a nontargeting (N/T) siRNA. Cells were treated with cycloheximide (CHX) for the indicated times and protein extracts were then immunoblotted for the indicated proteins. Long (l. e.) and short (s. e.) exposures are shown for KBP. f. Schematic representation of *Fbxo15* genomic locus and gRNA target location. Exon 1 refers to mouse *Fbxo15* gene in NC_000084.6 Reference GRCm38.p4 C57BL/6J and in NM_015798.3. In the bottom panel, full-length wild-type genomic DNA template and truncated mutant sequences identified by TOPO-TA cloning of *Fbxo15* PCR from two independent mESCs knockout clones are depicted. Clone #1 sequence and chromatogram revealed two different deletion events; one allele contains a 31bp deletion, while the other allele contains a 16bp deletion. Clone #2 sequence and chromatogram identified a 14bp deletion event at both alleles. Unprocessed original scans of blots are shown Supplementary Fig. 9. Unless otherwise noted, experiments were performed at least three times.

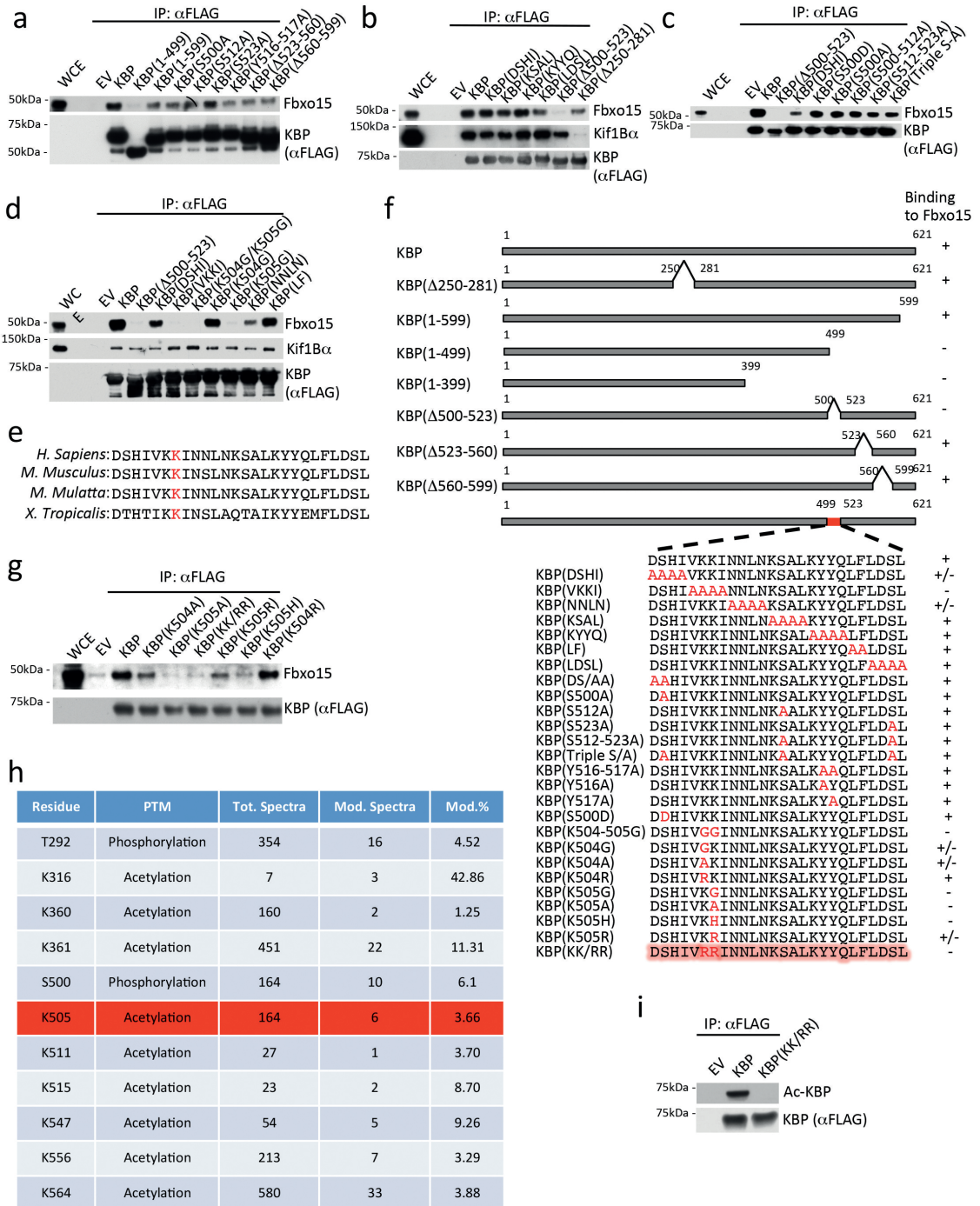

Residue	PTM	Tot. Spectra	Mod. Spectra	Mod.%
T292	Phosphorylation	354	16	4.52
K316	Acetylation	7	3	42.86
K360	Acetylation	160	2	1.25
K361	Acetylation	451	22	11.31
S500	Phosphorylation	164	10	6.1
K505	Acetylation	164	6	3.66
K511	Acetylation	27	1	3.70
K515	Acetylation	23	2	8.70
K547	Acetylation	54	5	9.26
K556	Acetylation	213	7	3.29
K564	Acetylation	580	33	3.88

Supplementary Figure 2 Identification of the KBP degron. a-d. HEK293T cells were transfected with either an empty vector (EV), wild type human KBP, or the indicated FLAG-tagged human KBP mutants (either deletion, truncation, or point mutation mutants, as indicated). Whole cell extracts (WCE) were immunoprecipitated (IP) with an anti-FLAG resin, and immunoprecipitates were probed with the indicated antibodies. e. Alignment of the Fbxo15 binding motif in KBP orthologs. The critical lysine required for Fbxo15 binding is highlighted in red. f. Schematic representation of KBP mutants. KBP mutants found to interact with Fbxo15 are indicated by the symbol (+). (+/-) denotes reduced binding, and (-) denotes a lack of binding. g. HEK293T cells were transfected with either an empty vector (EV), wild type human KBP, or the indicated FLAG-tagged human KBP point mutation mutants. Whole cell extracts (WCE) were immunoprecipitated (IP) with an anti-FLAG resin, and immunoprecipitates were probed with the indicated antibodies. h. Strep-FLAG-tagged human KBP was immunoprecipitated from HEK293T cells and subjected to PTM analysis. The table lists the number of spectra matching acetylated and phosphorylated peptides as a fraction of the total spectra detected for peptides bearing each modified residue and their corresponding modification percentage. This experiment was performed once. i. HEK293T cells were transfected with either an empty vector (EV) or vectors expressing FLAG-tagged wild type human KBP or FLAG-tagged human KBP(KK/RR). Whole cell extracts were immunoprecipitated (IP) with anti-FLAG resin, and proteins were immunoblotted as indicated. Unprocessed original scans of blots are shown Supplementary Fig. 9. Unless otherwise noted, experiments were performed at least three times.

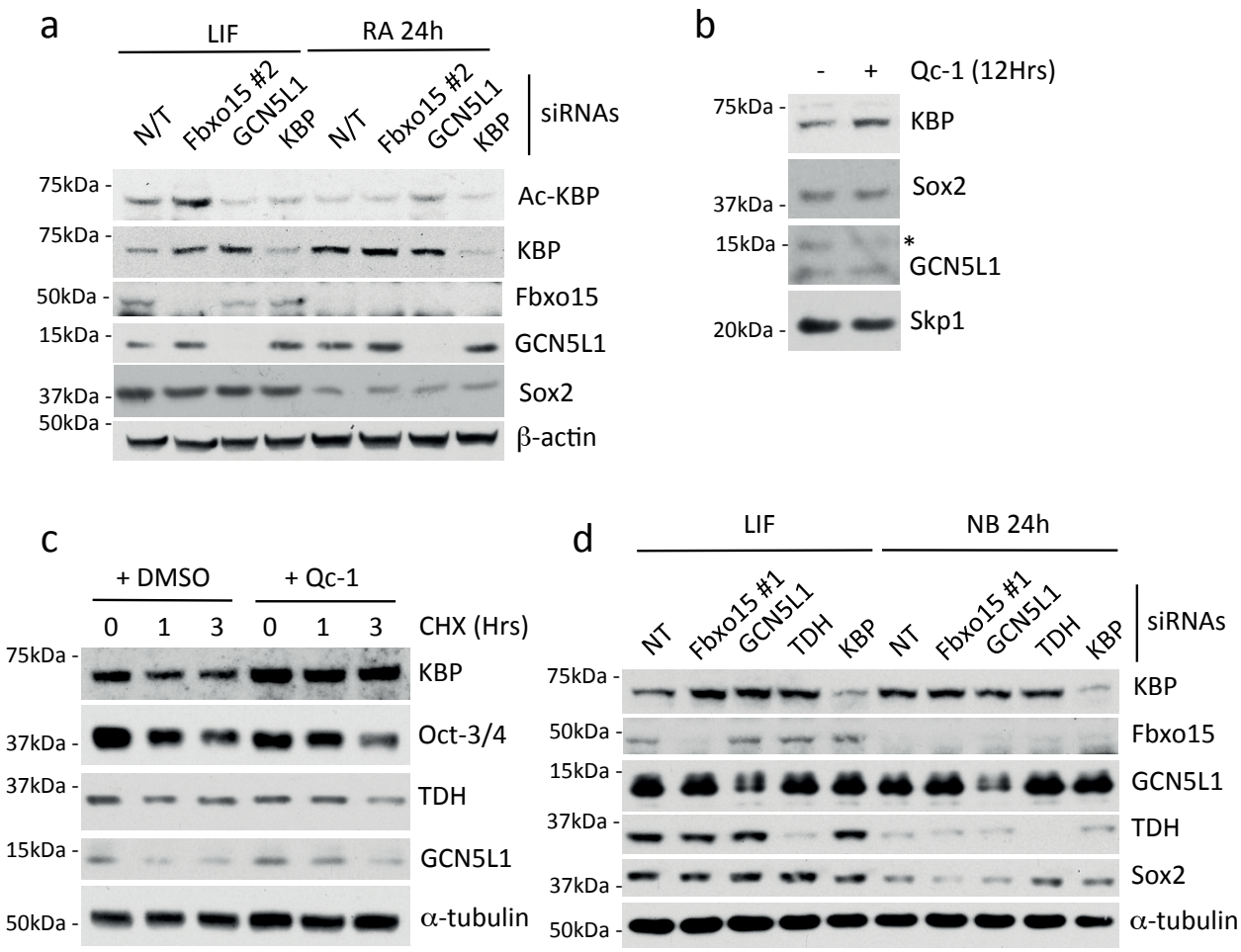

Supplementary Figure 3 GCN5L1 and TDH allow KBP degradation via Fbxo15. a. mESCs were transfected with either a nontargeting (N/T) siRNA or siRNAs to Fbxo15 (oligo #2), GCN5L1, or KBP. Cells were either maintained in LIF-containing medium or induced to differentiate for 24 hours after LIF withdrawal and exposure to retinoic acid (RA). Cells were then collected and lysed for immunoblotting as indicated. b. mESCs were treated for 12h with either DMSO or the TDH inhibitor Qc-1. Protein extracts were then immunoblotted for the indicated proteins. c. The experiment was performed as in (*b*), except that cells were treated with cycloheximide (CHX) for the indicated times. d. mESCs were transfected with either a nontargeting (N/T) siRNA or siRNAs to Fbxo15 (oligo #1), GCN5L1, KBP, or TDH. Cells were either maintained in LIF-containing medium or induced to differentiate for 24 hours after LIF withdrawal and exposure to neurobasal (NB) medium on non-adherent petri dishes. Cells were then collected and lysed for immunoblotting as indicated.Unprocessed original scans of blots are shown Supplementary Fig. 9. Unless otherwise noted, experiments were performed at least three times.

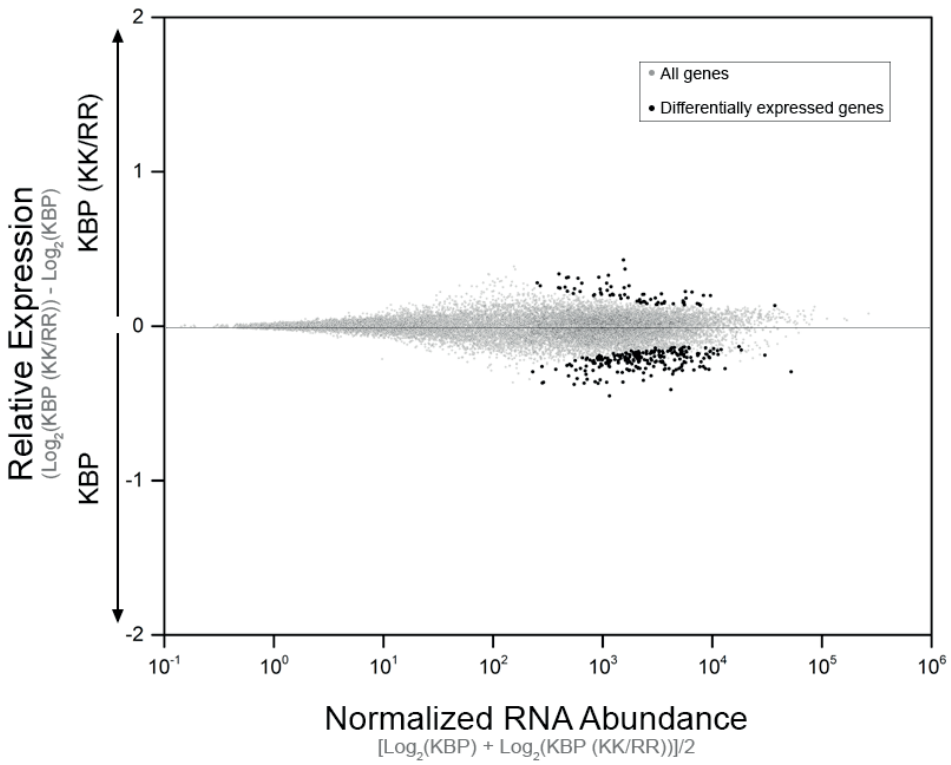

Supplementary Figure 4 Accumulation of KBP does not induce any major transcriptional rearrangement. mESCs were infected with lentiviruses expressing either HA-tagged wild type mouse KBP or HA-tagged mouse KBP(KK/RR) and maintained in self renewing conditions. RNA-seq analysis was performed and results are shown as a MA plot of log2 fold changes versus the mean of normalized counts. Genes were considered differentially expressed when the *p* adjusted value was <0.05. ~290 genes displayed differential expression, with modest fold changes (the relative expression for each affected transcript is comprised between -0.2 and +0.3). Neither a variation in the expression of the pluripotency core factors nor changes in the major metabolic drivers were detected. The complete list of FPKM reads is reported in Supplementary Table 2. n=3 biologically independent experiments.

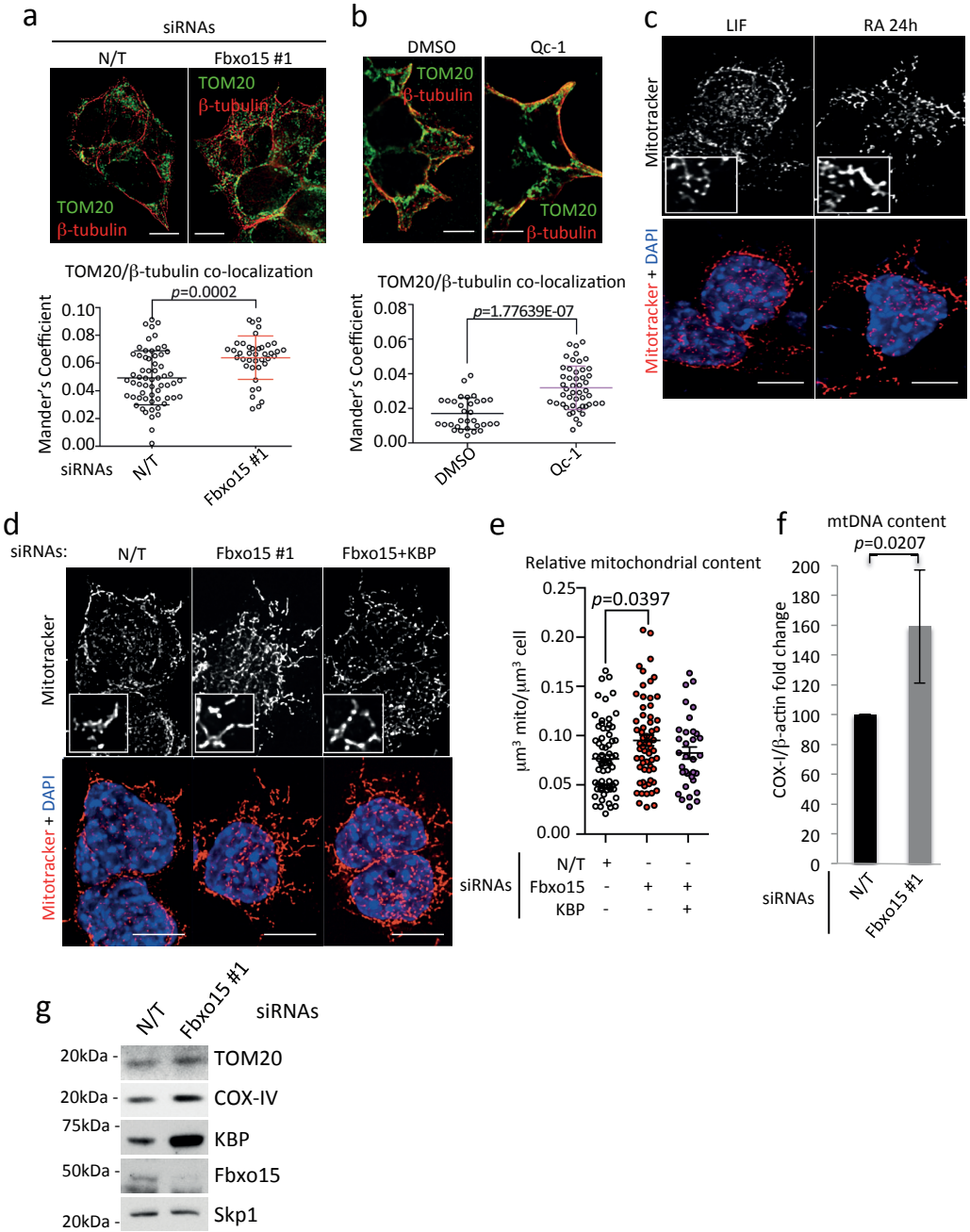

Supplementary Figure 5 Inhibition of KBP degradation promotes mitochondria-to-microtubule interaction and mitochondrial network expansion in mESCs. a. mESCs were transfected with either a nontargeting (N/T) siRNA or an siRNA to Fbxo15 (oligo #1) and immunostained for TOM20 and β-tubulin. Microtubule-mitochondria co-localization was detected using confocal microscopy. Scale bar = 15 µm. In the bottom graph, the Manders' Overlap Coefficient is shown. n=61 and 40 cells (N/T and Fbxo15 siRNA, respectively). *p* value was calculated by unpaired t-test. Error bars indicate +/-SD. b. mESCs were treated for 12 hours with DMSO or Qc-1 and immunostained for TOM20 and β-tubulin. Microtubule-mitochondria co-localization was detected by confocal microscopy. Scale bar = 15 µm. In the bottom graph, the Manders' Overlap Coefficient is shown. n=32 and 47 cells (DMSO and Qc-1 treatment, respectively). *p* values were calculated by unpaired t-test. Error bars indicate +/-SD. c. mESCs were either maintained in LIF-containing medium or induced to differentiate for 24 hours after LIF withdrawal and exposure to retinoic acid (RA). Cells were stained with Mitotracker and DAPI and then analyzed by 3D deconvolution microscopy. Representative MIPs are displayed. Scale bar = 15 µm. d-e. mESCs were transfected with either a nontargeting (N/T) siRNA or an siRNA to Fbxo15 (oligo #1) in the presence or absence of an siRNA to KBP, and maintained in LIF-containing medium. Cells were stained with Mitotracker and DAPI prior to fixation and then analyzed by confocal microscopy. Panel *d* shows the MIPs of representative cells (scale bar = 15 µm). Panel *e* shows the quantification of average mitochondrial content. n=62, 62 and 33 cells (N/T, Fbxo15 and Fbxo15+KBP siRNA, respectively). *p* value was calculated by one-way ANOVA. Error bars indicate +/-SD. f. mESCs were transfected with either an siRNA to Fbxo15 (oligo #1) or a nontargeting (N/T) siRNA. Total cellular DNA was extracted and mtDNA copy number was evaluated by qPCR normalized using b-actin DNA copy number. mtDNA amount in mESCs expressing transfected with a nontargeting (N/T) siRNA was set as 100 and the graph shows the fold change. *p* value was calculated by t-test. Error bars indicate +/-SD. n=4 biologically independent experiments (see Supplementary Table 6). g. mESCs were transfected with either an siRNA to Fbxo15 (oligo #1) or a nontargeting (N/T) siRNA. Protein extracts were then immunoblotted for the indicated proteins. Unprocessed original scans of blots are shown Supplementary Fig. 9. Unless otherwise noted, experiments were performed at least three times.

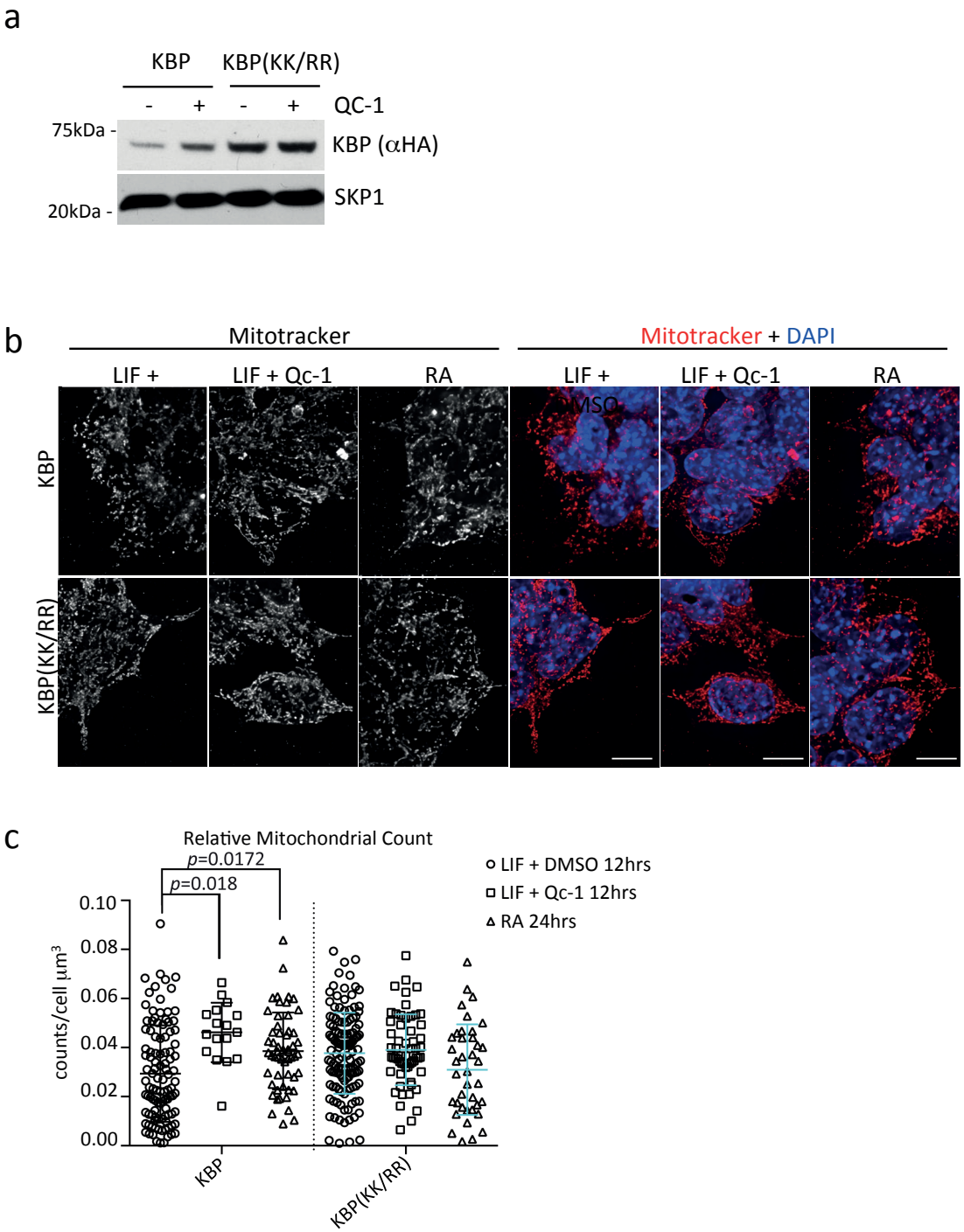

Supplementary Figure 6 Inhibition of KBP degradation induces a gain in mitonchondrial mass similar to that observed during differentiation. a. mESCs stably infected with lentiviruses expressing either HA-tagged wild type mouse KBP or HA-tagged mouse KBP(KK/RR) were treated for 12 hours with Qc-1. Cells were collected and lysed for immunoblotting as indicated. b-c. mESCs infected with lentiviruses expressing either HA-tagged wild type mouse KBP or HA-tagged mouse KBP(KK/RR) were either maintained in LIF-containing medium or induced to differentiate for 24h after LIF withdrawal and exposure to retinoic acid (RA). Where indicated, cells were treated for 12h with the TDH inhibitor Qc-1. Panel *b* shows the MIPs of representative cells (scale bar = 15 µm). Panel *c* shows the quantification of average mitochondrial count. Error bars indicate +/-SD. n=108, 17, 56, 129, 66 and 39 cells [KBP – DMSO, Qc-1 and differentiation - and KBP(KK/RR) – DMSO, Qc-1 and differentiation -, respectively]. *p* value was calculated by two-way ANOVA and multiple comparison. Unprocessed original scans of blots are shown Supplementary Fig. 9. Unless otherwise noted, experiments were performed at least three times.

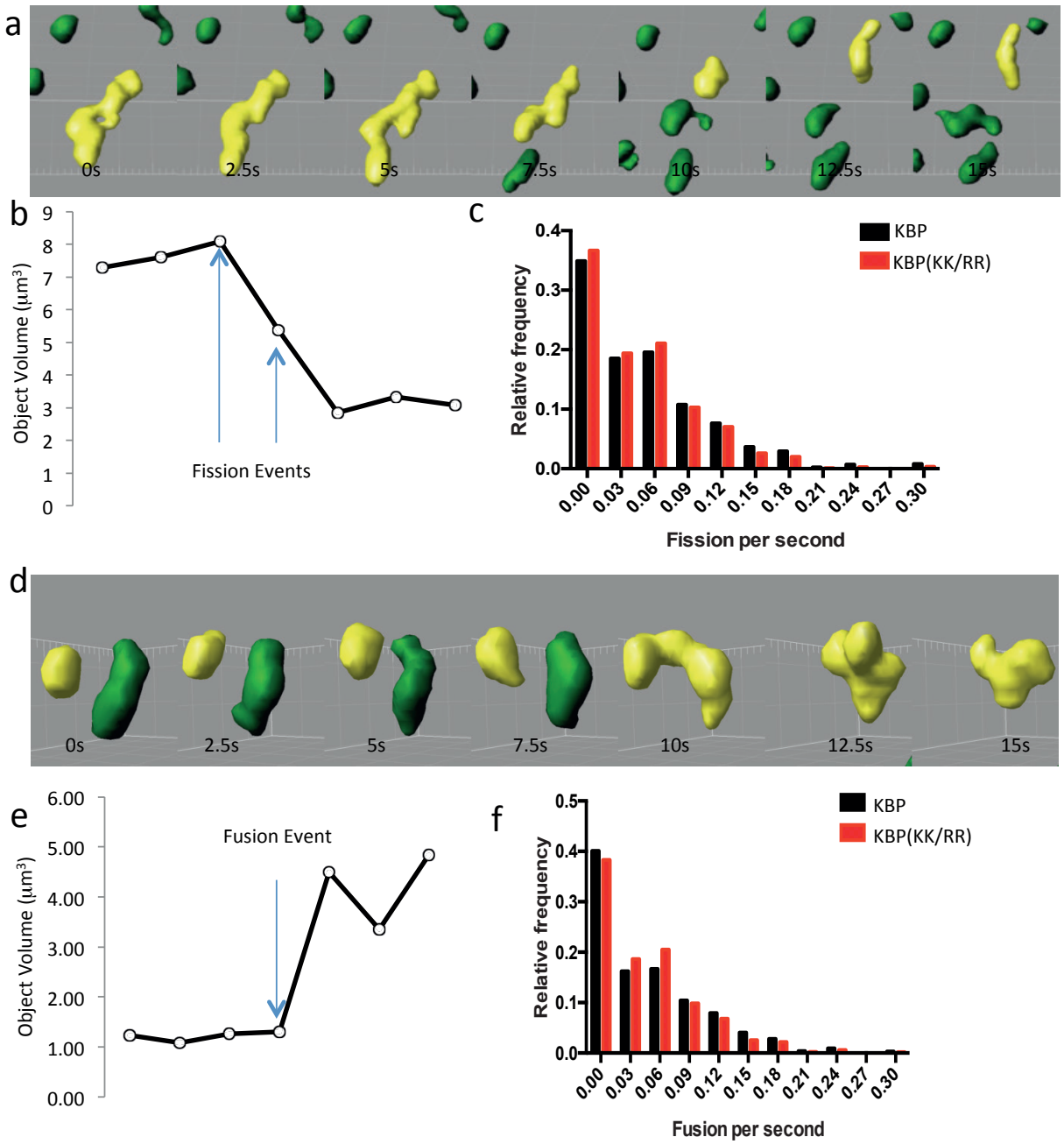

Supplementary Figure 7 Defects in KBP degradation do not affect mitochondrial dynamics. a-f. mESCs were infected with lentiviruses expressing either HA-tagged wild type mouse KBP or HA-tagged mouse KBP(KK/RR) and then transiently transfected with a plasmid expressing mitochondrial-targeted GFP. Panels *a* and *d* show representative 3D reconstructions of the mitochondria. Panels *b* and *e* show the entity of mitochondrial size changes registered in *a* and *d*, respectively. Panels *c* and *f* show the quantification of the events of mitochondrial fission and fusion. n=6 and 7 independent field acquisitions [KBP and KBP(KK/RR), respectively]. Statistics was calculated with unpaired t-test. This experiment was performed once.

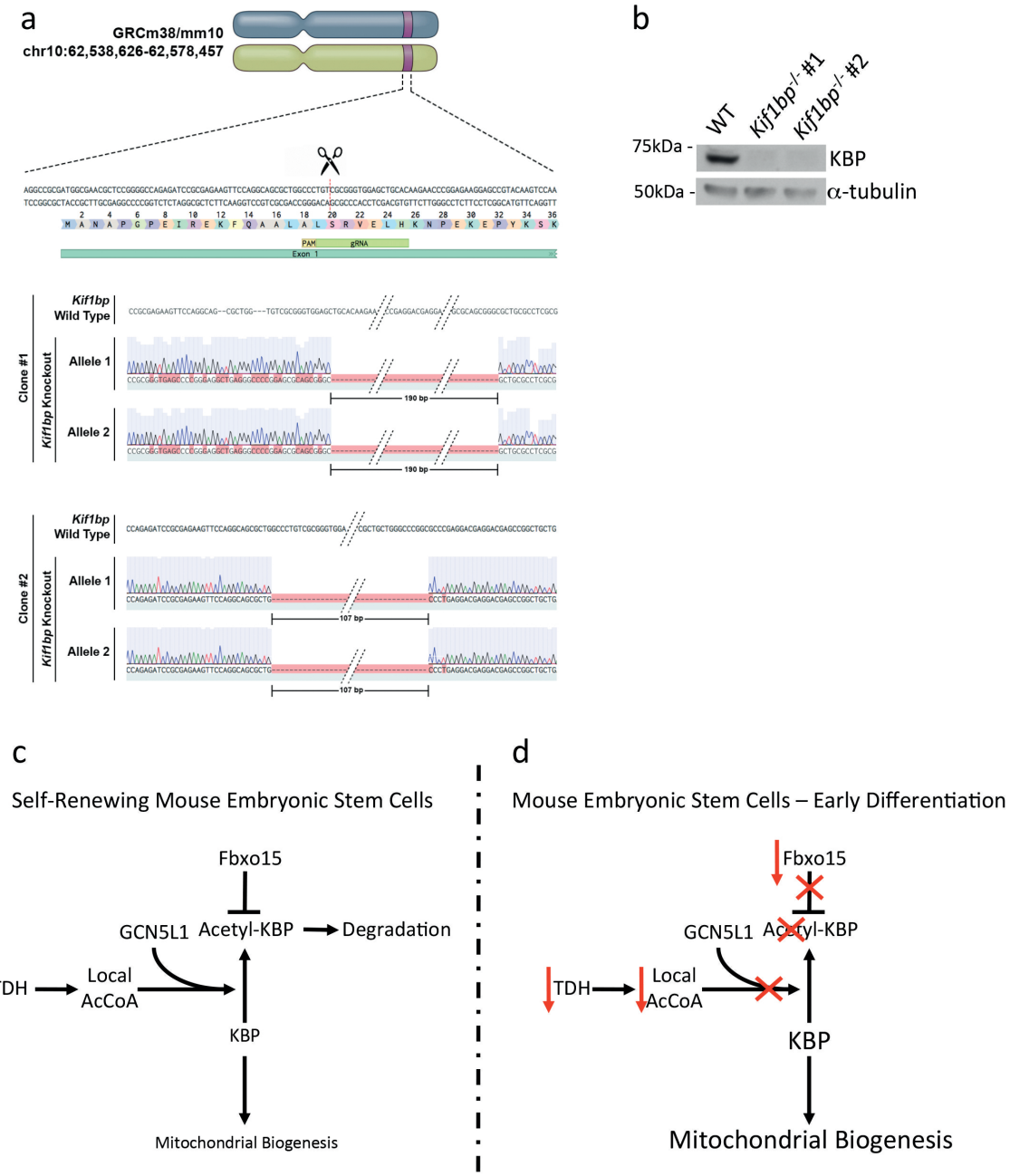

Supplementary Figure 8 Generation of *Kif1bp* $^{-/-}$ mESCs and model of regulation of mitochondrial biogenesis in mESCs. a. Generation of *Kif1bp*$^{-/-}$ mESCs by CRISPR Genome Editing. Schematic representation of *Kif1bp* genomic locus and gRNA target location. Exon 1 refers to mouse *Kif1bp* gene in NC_000076.6 Reference GRCm38.p4 C57BL/6J and in NM_028197.2. In the bottom panel, full-length wild-type genomic DNA template and truncated mutant sequences identified by TOPO-TA cloning of *Kif1bp* PCR from two independent mESCs knockout clones are depicted. Clone #1 sequence and chromatogram revealed an identical indel event at both alleles. Clone #2 sequence and chromatogram identified a 107bp deletion event at both alleles. b. Protein extracts from wild type mESCs (WT) and *Kif1bp-/-* mESCs (two different clones) were immunoblotted for the indicated proteins. Unprocessed original scans of blots are shown Supplementary Fig. 9. This experiment was performed three times. c. The TDH-dependent production of acetyl-CoA at mitochondria of naïve mESCs promotes the GCN5L1-mediated acetylation of KBP on Lysine 501. This event, in turn, allows KBP to be recognized by and degraded via Fbxo15, attenuating mitochondrial biogenesis during self-renewal. This molecular mechanism limits the accumulation of mitochondrial mass in self-renewing mESCs and preserves their optimal fitness. In human, *TDH* is an expressed pseudogene, a unique case among all metazoans (including chimpanzees) whose genomes have been sequenced to date (Pruitt *et al. Nucleic Acids Res.* 2007). However, the fact that the degron of KBP is conserved and acetylated in humans, together with the finding that its presence is necessary for KBP binding to Fbxo15, suggests that AcetylCoA is necessary for Fbxo15-mediated degradation of KBP in human cells as well, even if the source of AcetylCoA is different. Altogether, our data suggest that the molecular mechanism we have identified in mouse, with some minor differences, is conserved in humans. d. Upon differentiation, levels of Fbxo15 and TDH decrease, acetylation of KBP on Lysine 501 is inhibited, and KBP levels accumulate. We hypothesize that this accumulation results in the increase in cellular mitochondrial mass, which contributes to the metabolic switch in differentiating cells.

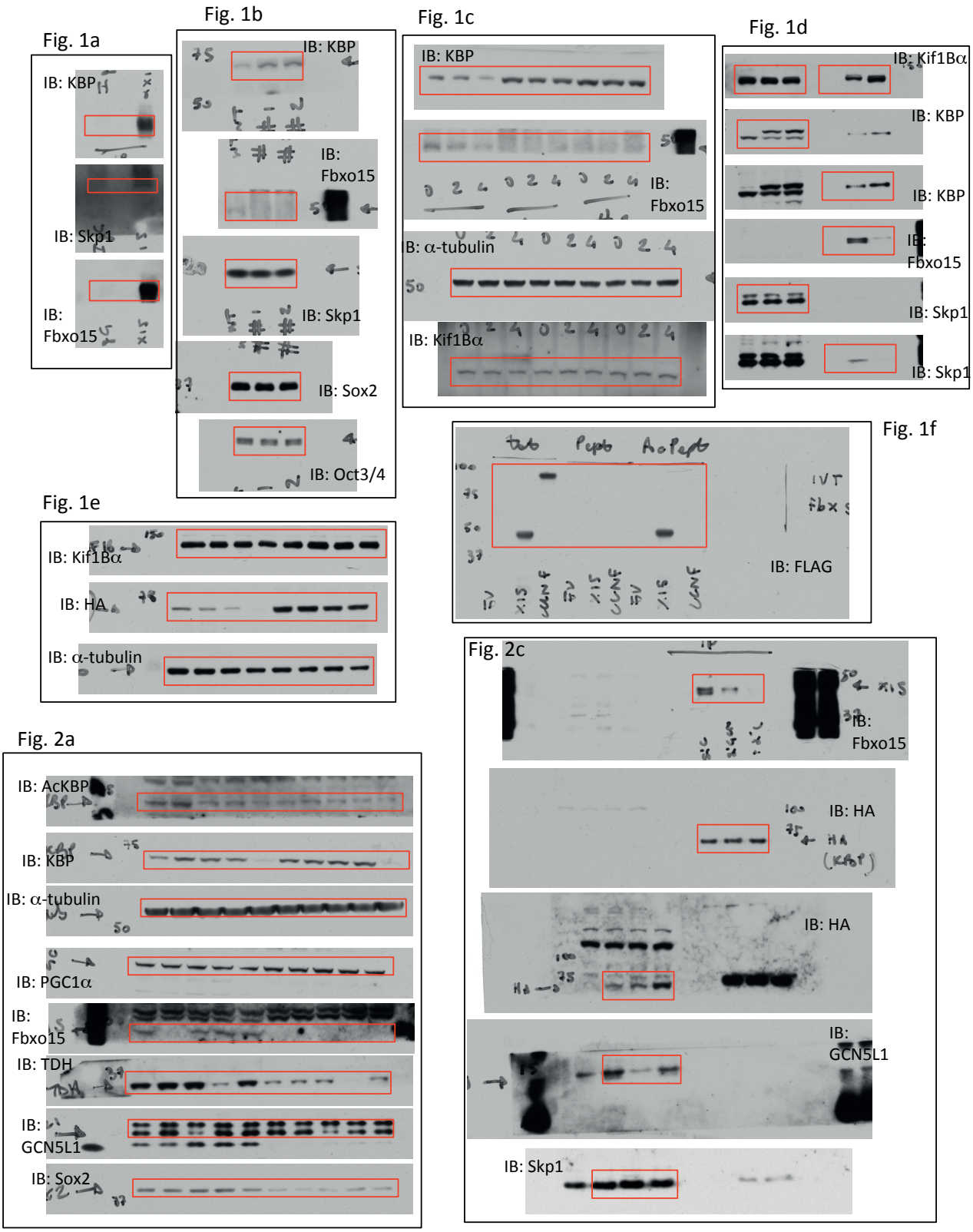

Supplementary Figure 9 Collection of the unprocessed blot scans used in this manuscript

Fig. 2b

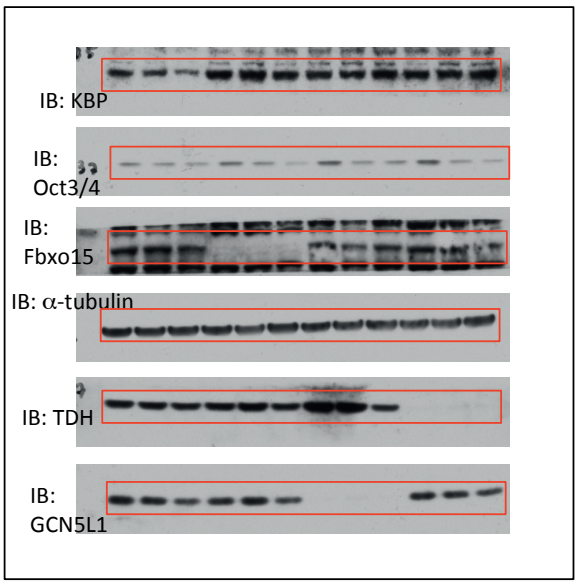

Fig. 2d

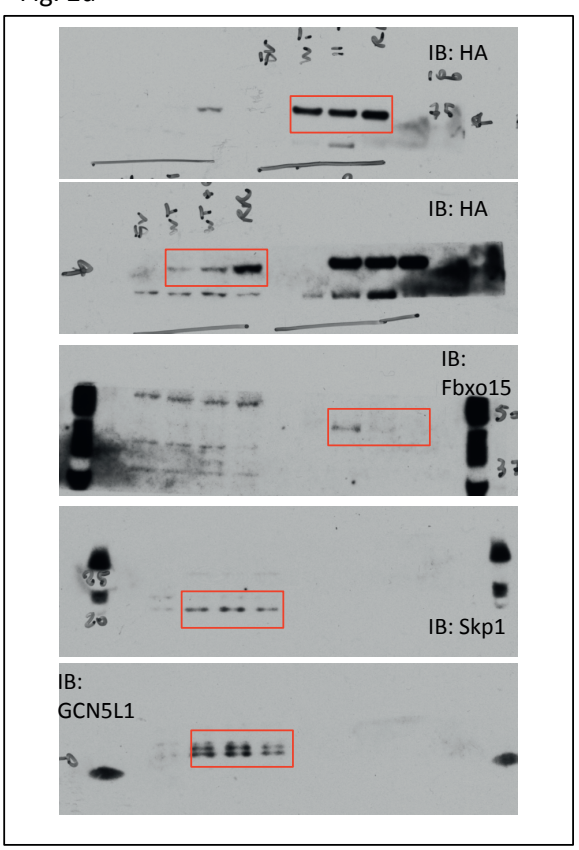

Fig. 3h

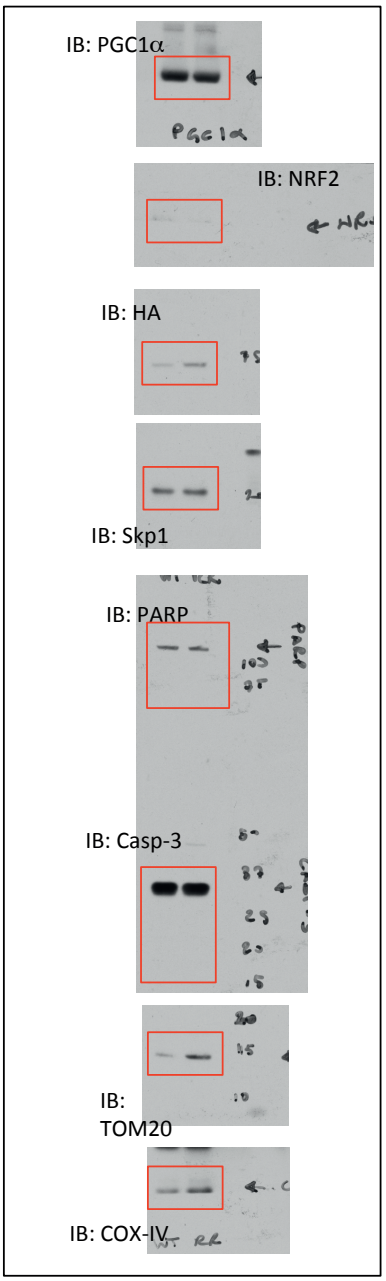

Supplementary Figure 9 Continued

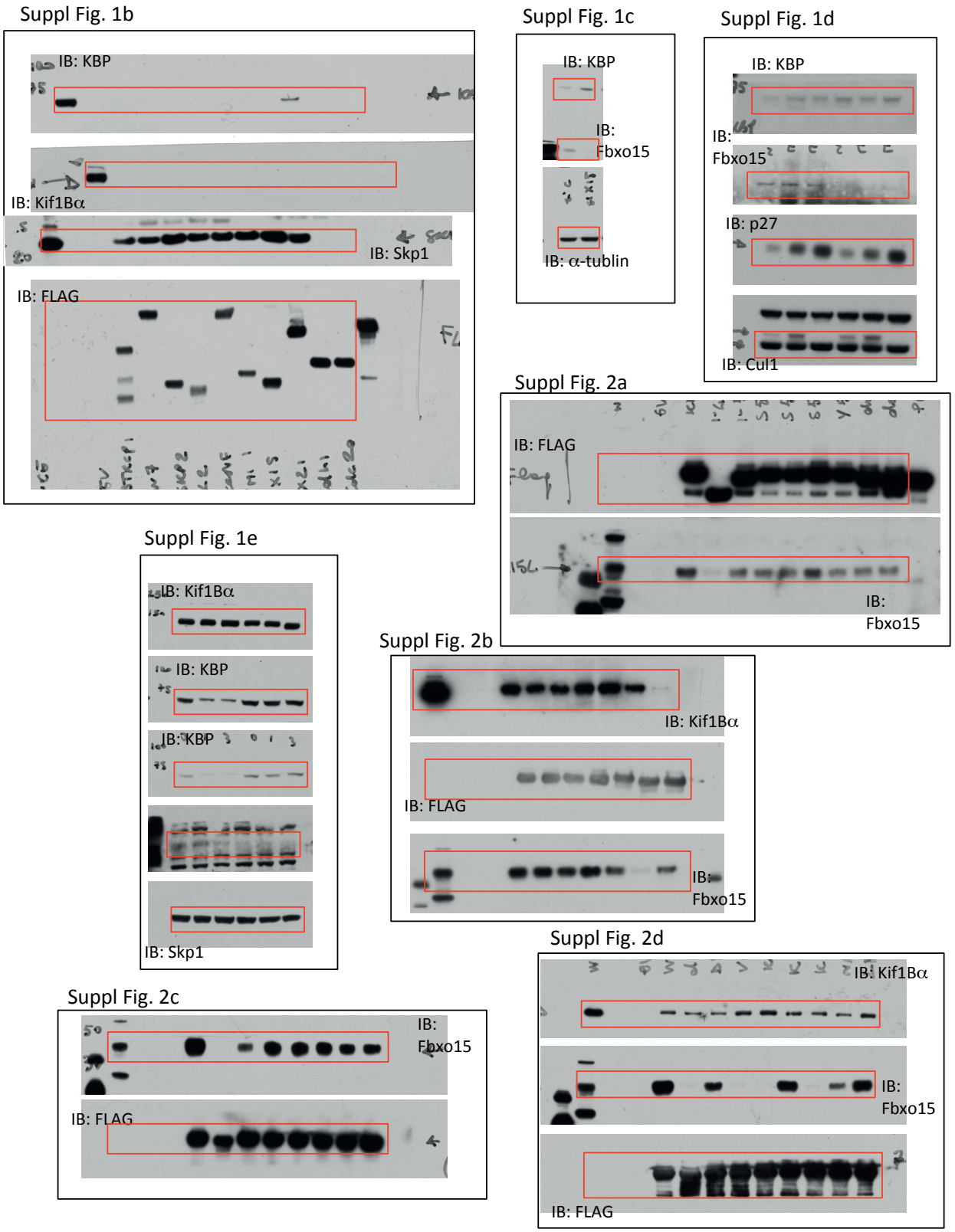

Supplementary Figure 9 Continued

Suppl Fig. 2g

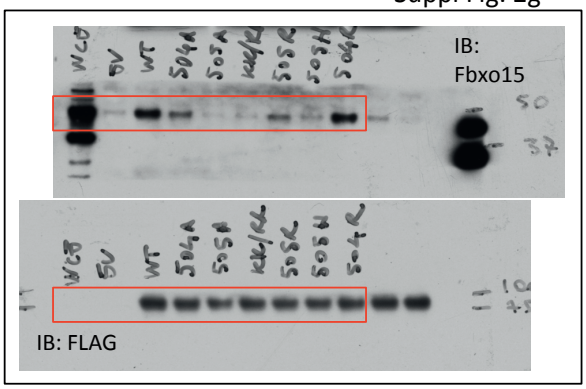

Suppl Fig. 2i

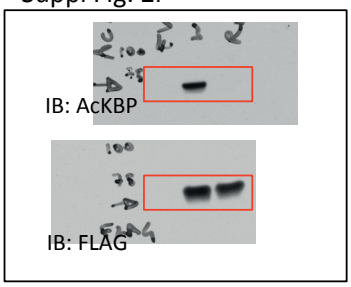

Suppl Fig. 3a

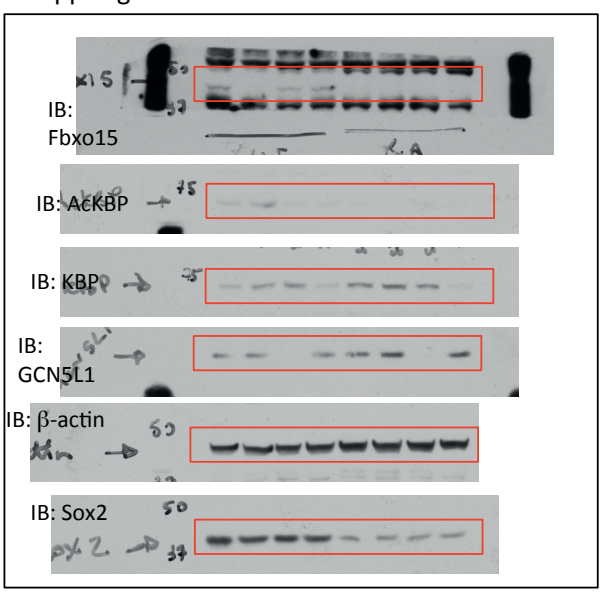

Suppl Fig. 3b

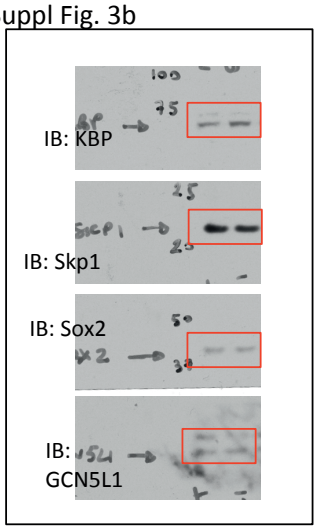

Suppl Fig. 3c

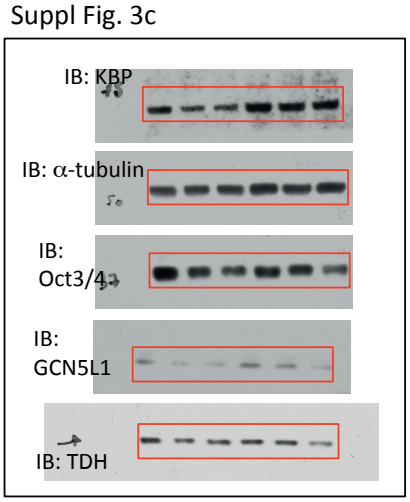

Suppl Fig. 3d

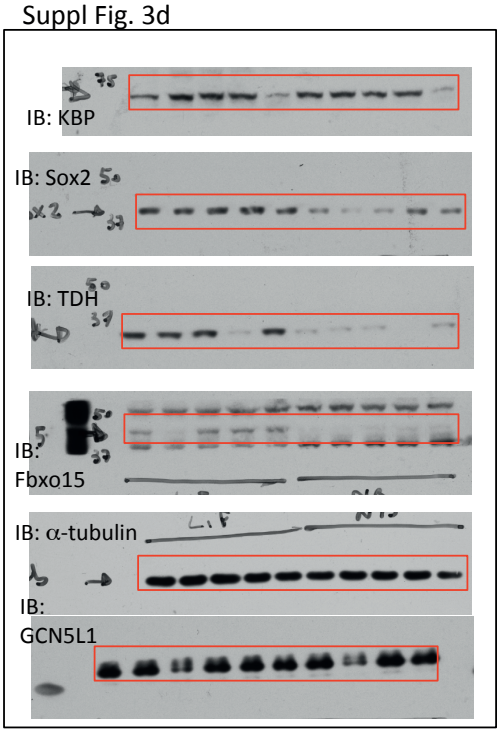

Supplementary Figure 9 Continued

Suppl Fig. 5g

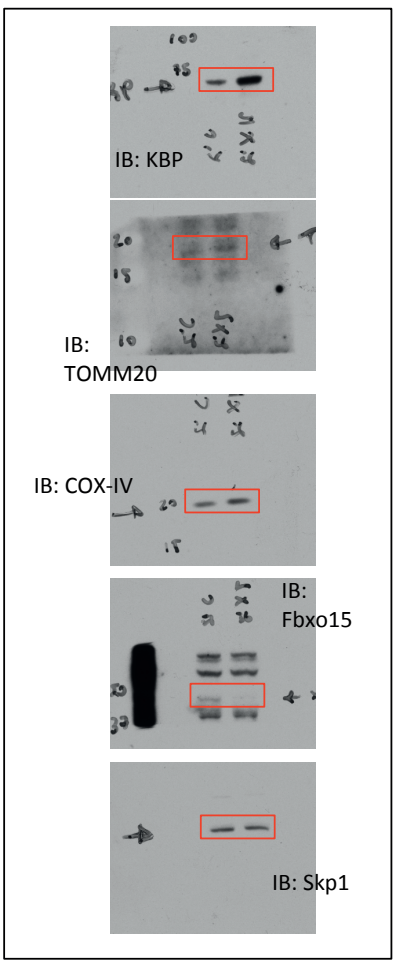

Suppl Fig. 6a

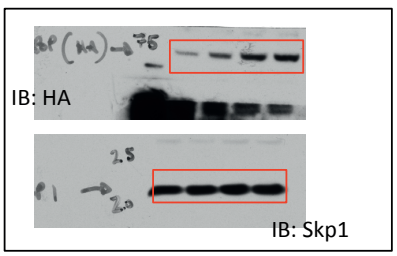

Suppl Fig. 8b

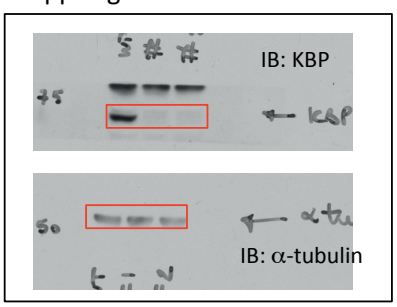

Supplementary Figure 9 Continued

Supplementary Table Legends

Supplementary Table 1 Multidimensional Protein Identification Technology analysis of the Fbxo15 complex. This table summarizes the list of proteins identified by MudPIT analyses of two Fbxo15 purifications, compared to an empty-vector control group, and filtered from contaminants reported in the CRAPome.

Supplementary Table 2 RNA-seq analysis in mESCs expressing either wild type KBP or a KBP stable mutant. Full list of FPKM reads obtained from the RNA sequencing of mESCs that were infected with lentiviruses expressing either HA-tagged wild type mouse KBP or HA-tagged mouse KBP(KK/RR), and maintained in self renewing conditions.

Supplementary Table 3 RNA-seq analysis in wild type and *Kif1bp*$^{-/-}$ embryoid bodies. FPKM list of transcripts that were up-regulated or down-regulated in embryoid bodies generated from either wild type or *Kif1bp*$^{-/-}$ mESCs.

Supplementary Table 4 Summary of Gene Ontology pathways that were downregulated in *Kif1bp*$^{-/-}$ embryoid bodies. The table summarizes the PANTHER Overrepresentation Test obtained by the analysis of transcripts that were significantly downregulated in embryoid bodies generated from *Kif1bp*$^{-/-}$ mESCs.

Supplementary Table 5 Sequences of primers, siRNA oligos, and gRNAs used in this manuscript.

Supplementary Table 6 Statistics source data.